Selective mass scaling for distorted solid-shell elements in explicit dynamics: optimal scaling factor and stable time step estimate

G. Cocchetti[1], M. Pagani[2], U. Perego[1*]

[1]*Department of Civil and Environmental Engineering, Politecnico di Milano, P.zza L. da Vinci, 32, 20133 Milano, Italy.*
[2]*Comsol S.r.l., v.le Duca degli Abruzzi 103, 25124 Brescia, Italy.*

SUMMARY

The use of solid-shell elements in explicit dynamics has been so far limited by the small critical time step resulting from the small thickness of these elements in comparison with the in-plane dimensions. To reduce the element highest eigenfrequency in inertia dominated problems, the selective mass scaling approach previously proposed in [G. Cocchetti, M. Pagani and U. Perego, *Comp. & Struct.* 2013; 127:39-52.] for parallelepiped elements is here reformulated for distorted solid-shell elements. Two objectives are achieved: the critical time step is governed by the smallest element in-plane dimension and not anymore by the thickness; the mass matrix remains diagonal after the selective mass scaling. The proposed approach makes reference to one-Gauss point, trilinear brick element, for which the maximum eigenfrequency can be computed analytically. For this element it is shown that the proposed mass scaling can be interpreted as a geometric thickness scaling, obtaining in this way a simple criterion for the definition of the optimal mass scaling factor. A strategy for the effective computation of the element maximum eigenfrequency is also proposed. The considered mass scaling preserves the element translational inertia, while it modifies the rotational one, leading to errors in the kinetic energy when the motion rotational component is dominant. The error has been rigorously assessed for an individual element and a simple formula for its estimate has been derived. Numerical tests, both in small and large displacements and rotations, using a state-of-the-art solid-shell element taken from the literature, confirm the effectiveness and accuracy of the proposed approach. Copyright © 2013 John Wiley & Sons, Ltd.

1. INTRODUCTION

Explicit time integration is often preferred for finite element nonlinear analyses of impulsively loaded shell structures. In view of the conditional stability of this type of integration algorithms, very small time steps are required for a stable time discretization, the step size being dictated by the smallest element dimension in the adopted mesh. On the other hand, explicit methods do not exhibit convergence problems and do not require the cumbersome and time consuming linearizations necessary in implicit methods, so that they are often preferred even when the load application is not particularly fast, in the presence of highly nonlinear problems, especially with contact and fracture. In these cases, analysis duration and small time step size, combined with time consuming internal force updating due to complex material models, soon lead to prohibitive computing costs.

*Correspondence to: umberto.perego@polimi.it, Department of Civil and Environmental Engineering, Politecnico di Milano, P.zza L. da Vinci, 32, 20133 Milano, Italy.

When the central difference integration scheme is used, a stable time step Δt must satisfy the condition

$$\Delta t \leq \frac{2}{\omega_{max}} \tag{1}$$

where ω_{max} is the maximum eigenfrequency of the assembled mesh. One also has that $\omega_{max} \leq \tilde{\omega}_{max} = \max_e\{\omega^e_{max}\}$, ω^e_{max} being the maximum eigenfrequency of an individual element of the mesh, so that a conservative time step bound is given by

$$\Delta t \leq \frac{2}{\tilde{\omega}_{max}} \tag{2}$$

According to Courant-Friedrichs-Levy, the stability condition may be rephrased saying that a stable time step must be smaller than the time required by a dilatational stress wave to traverse the smallest element in the mesh (*element traversal time*). i.e.

$$\Delta t \leq \frac{L^e}{c}, \quad c = \sqrt{\frac{\lambda + 2\mu}{\rho}} \tag{3}$$

where L^e is the smallest element dimension, λ and μ are Lame's constants, ρ is the mass density and c is the wave propagation speed.

The determination of the stable time step in (1) or (3) is based on the application of the central difference integration scheme to a model linear differential equation of motion. In the presence of material nonlinearities implying dissipation, the commonly used argument is that dissipation has a positive effect on stability, since it acts in the direction of reducing the propagation speed of stress dilatational waves within the mesh. A possibility in this case is to use the material tangent operator for a stability analysis of the linearized incremental problem. In this latter case, however, one has to take into account the possibility of elastic unloading, so that the elastic stable time step is normally used. Since in the presence of geometric nonlinearities, such as in large deformations, the physical process can be unstable, the definition of the stable time step in equation (1) is not rigorous, and a runtime test on energy is always recommended, together with a safety reduction factor, usually ranging between 0.8-0.98, to be applied to the used time step (see e.g. [1], chapt. 6).

From (2) and (3), one obtains that the maximum element eigenfrequency is strictly related to the smallest element dimension. This aspect is crucial in the analysis of shell structures, where the thickness can be significantly smaller than the surface dimensions. A heuristic remedy, which is often used, consists of artificially adding mass to the system so as to decrease the wave velocity and, hence, the maximum eigenfrequency. This can be easily obtained by uniformly increasing the material density (*uniform mass scaling*). The drawback of this provision is that all structural eigenmodes are affected by the mass increase, and not just those associated to the highest eigenfrequencies, altering in this way the dynamic structural response.

When classical or degenerated shell elements, i.e. elements based on middle surface displacement and rotation degrees of freedom (dofs), are used in conjunction with lumped mass matrices, a larger stable time step is usually obtained by artificially increasing the inertia associated to rotational degrees of freedom [2, 3] (see also [4]). Conversely, the inertia associated to middle plane nodal displacements is not altered, so that the element inertia associated to translational rigid body motions is not modified, which represents the basic requisite for the preservation of the most significant part of the dynamic structural response in inertia dominated problems. This way of proceeding is currently defined *selective mass scaling*, i.e. the element mass is artificially increased only for selected dofs.

Solid shell elements, i.e. shell elements based on solid elements kinematics, therefore making use of displacement degrees of freedom only, are becoming increasingly popular in view of the computational advantages that they can provide in some applications (see e.g. [5, 6, 7, 8]). However, these elements exhibit an inherently bad aspect ratio due to the small thickness compared to the in-plane dimensions. For this reason, they are preferably used in implicit dynamics approaches, to avoid the small critical time step produced by the high maximum eigenfrequency, and only recently their usage in explicit dynamics approaches seems to have been attracting a specific attention (see

e.g. [7, 9, 10, 11]). Systematic studies on the computational effectiveness of solid-shell elements in explicit dynamics have also been recently presented in [12, 13].

Since solid-shell elements do not make use of rotational dofs, direct application of the selective mass scaling proposed in [2, 3] is not possible. Another possibility to reduce the element highest eigenfrequency is to modify the mass matrix by adding to it the stiffness matrix multiplied by a scaling parameter [14, 15]. It can be shown that in this way the highest eigenfrequencies can be reduced with negligible modifications of the lowest ones. In particular, this type of scaling leaves the inertia forces unmodified for rigid body motions, since in this case no internal forces are produced. As in large deformation problems the stiffness matrix changes during the deformation process, in [15] it has been proposed to add to the stiffness matrix a suitably constructed constant matrix producing zero inertia forces for rigid body translations. Other mass scaling techniques have been discussed in [16], while a new bipenalty approach, whereby both the stiffness and the mass matrix are selectively scaled, has been proposed in [17]. A rigorous variational framework has been presented in [18], where different types of selective mass scaling formulations, preserving both translational and rotational inertia in rigid body motions, are obtained from a penalized mixed Hamilton's principle. In the functional, displacements, velocities and momenta appear as independent fields and are discretized using different trial functions. The relations between the three fields are enforced by means of penalization factors in the functional. It is shown how the approach in [15] can be obtained as a special case, therefore proving its variational consistency. At the same time, other forms of selectively scaled consistent mass matrices are derived, which are shown to provide superior performances in the investigated examples. Both local and global selective mass scaling strategies, have been studied in [19]. Rigorous criteria for optimality have been formulated, both in terms of accuracy and in terms of computational effectiveness in the case of linearized elasto-dynamics and a mass scaling preserving eigenmodes while leading to only small fill-in of the scaled mass matrix has been proposed.

A common problem of all these formulations is that they lead to a non-diagonal mass matrix, thus compromising the fully explicit nature of the algorithm. The issue of preserving the diagonal structure of the mass matrix after selectively scaling its entries has been addressed in [20]. Starting from a classical 8-node brick element with trilinear displacement interpolation, the solid-shell displacement dofs are linearly transformed into *average* displacements (i.e. representing displacements of the middle surface) and *difference* displacements (i.e. representing the difference between displacements of the shell upper and lower surfaces). The resulting element is kinematically equivalent to the original brick and possesses the same eigenfrequencies. The advantage is that it is now possible to artificially increase the masses pertinent to the *difference* dofs while leaving unaltered those relative to the *average* ones. In this way, the inertia of the resulting element associated to translational rigid body motions does not change, while the highest eigenfrequencies decrease. In the case of an arbitrarily distorted element, the mass matrix of the transformed element is not diagonal even when the mass matrix of the original element is lumped. However, it is almost diagonal (i.e. extra-diagonal entries are small if compared to the diagonal ones) so that it can be easily lumped. This mass scaling approach is conceptually similar to what is usually done with classical shell elements, as mentioned above, and to what has been proposed in [21] for solid-like shells. The advantage of the procedure proposed in [20] is that it provides a consistent transformation also for the stiffness matrix, allowing for the formulation of the element eigenvalue problem that is required for the accurate computation of the maximum eigenfrequency. The positive effects of the selective mass scaling approach presented in [20] have been assessed also in the study discussed in [13]. It is also worth mentioning the geometric scaling approach used in several works [22, 23, 24] to improve the conditioning of the stiffness matrix of thin solid-shells in implicit approaches and to reduce in this way the computational burden associated to the use of iterative solvers. In these works, the scaling consisted of increasing the thickness so as to make it reach a length comparable to the element in-plane dimensions. As it will be discussed later, selective mass scaling and thickness scaling can be shown to produce similar effects on the element highest eigenfrequency.

After mass scaling is applied, one remains with the problem of computing the largest stable time step, i.e. the largest element eigenfrequency, in an efficient way. For uniform density elements (i.e.,

without selective mass scaling), the largest eigenfrequency is usually estimated using Gershgorin's theorem [25], which provides a rigorous upper bound, or using one of the strategies specifically devised for explicit finite element applications (see e.g. [26, 27]). However, in [20] it has been shown that these simple estimates cannot be satisfactorily used when the mass matrix has been selectively scaled, since they lead to overly large upper bounds on the largest eigenfrequency. To address this issue, in [20] the eigenvalue problem of a solid-shell element of parallelepiped shape was solved analytically. For a parallelepiped, ω_{max}^e has been shown to correspond to the uniform *normal-strain* deformation mode [26] given by a uniform thickness contraction/expansion (assuming that the thickness is the element smallest dimension), while an analytical solution for an arbitrarily distorted element could not be achieved. The value computed for a parallelepiped was used to obtain a reasonable estimate also for slightly distorted elements, but for arbitrarily distorted solid-shell elements with selectively scaled masses, the problem of the determination of the maximum eigenfrequency remained open.

In explicit finite element analyses, elements based on reduced integration are preferred in most cases in view of their smaller computational cost. To better represent the bending behavior, in solid-shell elements reduced integration is applied only in in-plane directions, while several Gauss points are commonly used in thickness direction. Since reduced integration has the effect to reduce the element stiffness with respect to certain deformation modes, a modification of the eigenfrequency spectrum is expected when compared to the corresponding fully integrated element. In the case of arbitrarily distorted elements, simple estimates of the element maximum eigenfrequency have been provided in [26] for uniform density, constant strain (i.e. with one quadrature point) quadrilaterals and hexahedra. However, these estimates are not accurate enough when masses are selectively scaled and need be revised.

The selective mass scaling approach proposed in [20] for parallelepiped or slightly distorted elements is here generalized to arbitrary distortions and its connection with element thickness scaling is shown in a rigorous way. A procedure for a computationally effective estimate of the largest eigenfrequency for a solid-shell element with masses selectively scaled according to this approach, is also proposed. The procedure closely follows the original approach of Flanagan and Belytschko [26] for constant strain brick elements, adapting it to the case of scaled masses.

The considered mass scaling preserves the element translational inertia, while it modifies the rotational one, leading to errors in the kinetic energy when the motion rotational component is dominant. The error has been rigorously assessed for an individual element and a simple formula for its estimate has been derived. In applying selective mass scaling, one also has to devise a strategy for the definition of the scaling parameter, accounting for the conflicting objectives of preserving accuracy (i.e. small scaling) and maximizing the critical time step (i.e. large scaling). This issue has been dealt with in [13], where a simple empirical strategy has been proposed, based on the asymptotic computation of the maximum eigenfrequency that would be obtained for an infinite value of the scaling parameter. The issue of the definition of the optimal choice of the scaling parameter is also discussed in this paper and a simple procedure is proposed, which exploits the analogy between mass and geometric scalings. The approach is validated through numerical tests where the solid-shell element recently proposed in [28, 8] has been used as a reference.

1.1. Notation

The tensor double contraction symbol ":" will be used here in an unconventional way to denote the following matrix operation. Let $\mathbf{A}$ and $\mathbf{B}$ be two matrices with n rows and m columns. Then

$$\mathbf{A}_{n \times m} : \mathbf{B}_{n \times m} = \sum_{i=1}^{n} \sum_{j=1}^{m} A_{ij} B_{ij} = \mathbf{B} : \mathbf{A} \tag{4}$$

The following identity can then be easily verified:

$$\mathbf{A}_{n \times p} \mathbf{C}^T_{p \times m} : (\mathbf{B}_{n \times m}) = \mathbf{A} : (\mathbf{BC}) \tag{5}$$
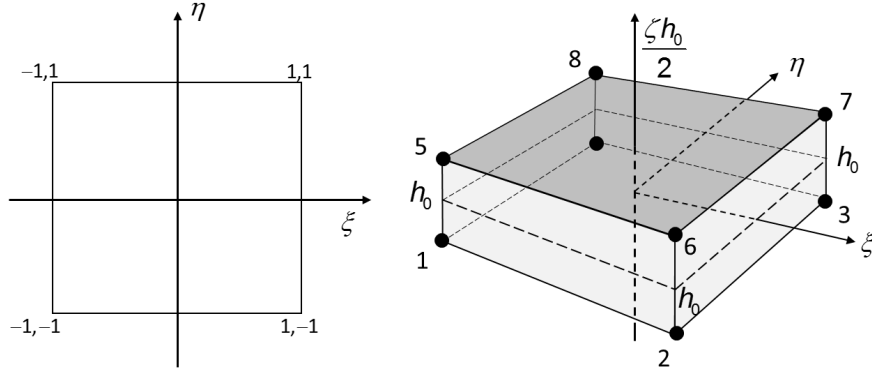
Figure 1. Reference parallelepiped element with square bases.

Setting $n = m$ and $\mathbf{B} = \mathbf{I}$, $\mathbf{I}$ being the $n \times n$ identity matrix, one recovers the matrix operation corresponding to the trace of a square matrix:

$$\underset{n \times p}{\mathbf{A}} : \underset{n \times p}{\mathbf{C}} = \mathbf{A}\mathbf{C}^T : \mathbf{I} \tag{6}$$

In analogy with the corresponding tensor notation, the single contraction symbol "·" will be used in the case of matrices having only one column ($m = 1$). Then, if $\mathbf{u}$ and $\mathbf{v}$ are column vectors with n rows, one has

$$\underset{n \times 1}{\mathbf{u}} \cdot \underset{n \times 1}{\mathbf{v}} = \sum_{i=1}^{n} u_i v_i = \underset{1 \times n}{\mathbf{u}^T} \underset{n \times 1}{\mathbf{v}} = \underset{1 \times n}{\mathbf{v}^T} \underset{n \times 1}{\mathbf{u}} \tag{7}$$

Furthermore, if one defines $\mathbf{v}_{n \times 1} = \mathbf{V}_{n \times m} \mathbf{N}_{m \times 1}$, one obtains

$$\underset{n \times 1}{\mathbf{u}} \cdot \underset{n \times 1}{\mathbf{v}} = \mathbf{u} \cdot (\mathbf{V}\mathbf{N}) = \underset{n \times 1}{\mathbf{u}} \underset{1 \times m}{\mathbf{N}^T} : \underset{n \times m}{\mathbf{V}} = \underset{m \times n}{\mathbf{V}^T} \underset{n \times 1}{\mathbf{u}} \cdot \underset{m \times 1}{\mathbf{N}} \tag{8}$$

Finally, the following notation will be used to denote surface and volume integrals in the element intrinsic coordinate space

$$\int_{\boxdot} d\xi d\eta d\zeta, \quad = \int_{-1}^{1} \int_{-1}^{1} \int_{-1}^{1} d\xi d\eta d\zeta, \quad \int_{\square} d\xi d\eta = \int_{-1}^{1} \int_{-1}^{1} d\xi d\eta \tag{9}$$

2. SELECTIVE MASS SCALING FOR SOLID-SHELL ELEMENTS

2.1. Element geometry

Solid-shell elements are solid brick elements characterized by a dimension, the thickness, which is smaller than the other two. In view of this geometric characteristics, it is here assumed that it is possible to unambiguously identify the element upper and lower faces. In the case of distorted elements, a more rigorous definition of the thickness principal direction will be given later in this section. The usual isoparametric geometry description will be adopted to account for element distortion with respect to the parent cube of size $2 \times 2 \times 2$.

Let $\boldsymbol{\xi}^T = [\xi, \eta, \zeta]$ be a set of intrinsic coordinates, with origin in the centroid of the parent cube and $\boldsymbol{\xi}_a$ the intrinsic coordinates of node a, $a = 1 \ldots 8$. Let $\boldsymbol{\xi}_{\boxdot}$ define the matrix collecting vectors $\boldsymbol{\xi}_a$, i.e.

$$\underset{3 \times 8}{\boldsymbol{\xi}_{\boxdot}} = [\boldsymbol{\xi}_1 \cdots \boldsymbol{\xi}_a \cdots \boldsymbol{\xi}_8] \begin{bmatrix} -1 & 1 & 1 & -1 & -1 & 1 & 1 & -1 \\ -1 & -1 & 1 & 1 & -1 & -1 & 1 & 1 \\ -1 & -1 & -1 & -1 & 1 & 1 & 1 & 1 \end{bmatrix}, \quad \boldsymbol{\xi}_{\boxdot} \boldsymbol{\xi}_{\boxdot}^T = 8\mathbf{I}_3 \tag{10}$$

where $\mathbf{I}_3$ is the 3×3 identity matrix. It is assumed that ζ is the coordinate in the thickness direction. Let $\mathbf{X}$ be the 3×8 matrix containing as columns the element nodal coordinates $\mathbf{X}_a$, $a = 1, \ldots 8$ with respect to a fixed reference frame

$$\underset{3 \times 8}{\mathbf{X}} = \left[\mathbf{X}_1 \cdots \underset{3 \times 1}{\mathbf{X}_a} \cdots \mathbf{X}_8 \right] = \left[\underset{3 \times 4}{\mathbf{X}_{1-4}} \ \underset{3 \times 4}{\mathbf{X}_{5-8}} \right] \tag{11}$$

Element nodes are ordered as shown in Figure 1, where a parallelepiped element with square bases is shown. The thickness is easily identified as the smallest dimension. Nodes 1-4 define vertices of the lower element surface, while nodes 5-8 define vertices of the upper one. The coordinates of a point belonging to an arbitrarily distorted element Ω^e can then be expressed through the geometry mapping

$$\underset{3 \times 1}{\mathbf{x}} (\boldsymbol{\xi}) = \underset{3 \times 8}{\mathbf{X}} \underset{8 \times 1}{\mathbf{N}} (\boldsymbol{\xi}), \quad \mathbf{N} = [N_1 \cdots N_a \cdots N_8]^T \tag{12}$$

where $N_a = \frac{1}{8}(1 + \xi \xi_a)(1 + \eta \eta_a)(1 + \zeta \zeta_a)$ are the usual trilinear interpolation functions. The element volume is given by

$$V = \int_{\Omega^e} d\Omega = \int_{\square} |\det[\mathbf{J}(\boldsymbol{\xi})]| d\xi d\eta d\zeta \tag{13}$$

where $\mathbf{J}(\boldsymbol{\xi})$ is the Jacobian matrix of the geometry mapping

$$\underset{3 \times 3}{\mathbf{J}} (\boldsymbol{\xi}) = \frac{\partial \mathbf{x}}{\partial \boldsymbol{\xi}^T} = \left[\frac{\partial \mathbf{x}}{\partial \xi} \ \frac{\partial \mathbf{x}}{\partial \eta} \ \frac{\partial \mathbf{x}}{\partial \zeta} \right] = \underset{3 \times 8}{\mathbf{X}} \underset{8 \times 3}{\frac{\partial \mathbf{N}}{\partial \boldsymbol{\xi}^T}} = \mathbf{X} \left[\frac{\partial \mathbf{N}}{\partial \xi} \ \frac{\partial \mathbf{N}}{\partial \eta} \ \frac{\partial \mathbf{N}}{\partial \zeta} \right] \tag{14}$$

Let the element distortion be interpreted as a deformation process from the parent cubic configuration to the current distorted geometry. In this way $\boldsymbol{\xi}$ and $\mathbf{x}$ represent the original and current configurations, respectively, while $\mathbf{J}(\boldsymbol{\xi})$ is the deformation gradient. The principal directions of the Cauchy deformation tensor $\mathbf{c} = \mathbf{J}^{-T} \mathbf{J}^{-1}$, corresponding to the inverse of the left Cauchy–Green (or Finger) deformation tensor $\mathbf{b} = \mathbf{J}\mathbf{J}^T$, define the directions of principal stretch in the current configuration.

Let

$$\mathbf{c} = \sum_{i=1}^{3} \gamma_i^2 \mathbf{t}_i \otimes \mathbf{t}_i \tag{15}$$

define the spectral decomposition of $\mathbf{c}$, with $\gamma_1^2 \leq \gamma_2^2 \leq \gamma_3^2$. The eigenvector $\mathbf{t}_3$ associated to the maximum eigenvalue γ_3^2 defines the direction of maximum shortening in the current configuration. Since it is assumed that the element thickness is significantly smaller than the in-plane dimensions, $\mathbf{t}_3$ locally defines the thickness direction, which however may vary from point to point within the same element. A unique definition is obtained in the case of an underintegrated element (one Gauss point), which will be considered in Section 3.2, since $\mathbf{J}^{-T} \mathbf{J}^{-1}$ becomes constant. In this case, $\mathbf{t}_3$ can be identified as the element principal thickness direction.

In shell elements it is convenient to express the geometry in terms of the element middle surface. For solid-shell elements this can be done by defining middle surface nodes of coordinates $\mathbf{X}^m$, where

$$\underset{3 \times 4}{\mathbf{X}}^m = \frac{\mathbf{X}_{1-4} + \mathbf{X}_{5-8}}{2} \tag{16}$$

It is also useful to define the element "fibers" as the segments connecting points corresponding to each other on the element upper and lower surfaces. Corner fibers are then defined as $2\Delta\mathbf{X}$ where

$$\underset{3 \times 4}{\Delta\mathbf{X}} = \frac{\mathbf{X}_{5-8} - \mathbf{X}_{1-4}}{2} \tag{17}$$

The relation between element nodal coordinates $\mathbf{X}$ and middle surface nodes and corner fibers coordinates gathered in matrix $\hat{\mathbf{X}}$ can be synthetically expressed defining the transformation

operator $\mathbf{Q}$:

$$\mathbf{X} = [\mathbf{X}_{1-4} \ \mathbf{X}_{5-8}] = \underset{3\times8}{\hat{\mathbf{X}}} \underset{8\times8}{\mathbf{Q}} = [\mathbf{X}^m \underset{3\times4}{\ } \underset{3\times4}{\Delta\mathbf{X}}] \left[\begin{array}{cc} \mathbf{I}_4 & \mathbf{I}_4 \\ -\mathbf{I}_4 & \mathbf{I}_4 \end{array} \right]$$

$$\hat{\mathbf{X}} = \frac{1}{2}\mathbf{X}\mathbf{Q}^T \quad \text{with} \quad \mathbf{Q}\mathbf{Q}^T = 2\mathbf{I}_8 \quad \text{and} \quad \mathbf{Q}^{-1} = \frac{1}{2}\mathbf{Q}^T \tag{18}$$

where $\mathbf{I}_4$ and $\mathbf{I}_8$ are the 4×4 and 8×8 identity matrices, respectively. The element geometry and the geometry mapping can also be expressed in terms of middle surface coordinates $\mathbf{X}^m$ and corner fibers $\Delta\mathbf{X}$

$$\mathbf{x}(\boldsymbol{\xi}) = \mathbf{X}\mathbf{N}(\boldsymbol{\xi}) = \hat{\mathbf{X}}\mathbf{Q}\mathbf{N}(\boldsymbol{\xi}) = \hat{\mathbf{X}}\hat{\mathbf{N}} \tag{19}$$

with

$$\underset{8\times1}{\hat{\mathbf{N}}}(\boldsymbol{\xi}) = \left[\begin{array}{c} \underset{4\times1}{\mathbf{N}^m(\boldsymbol{\xi})} \\ \underset{4\times1}{\Delta\mathbf{N}(\boldsymbol{\xi})} \end{array} \right] = \mathbf{Q}\mathbf{N}(\boldsymbol{\xi}) = \left[\begin{array}{c} \mathbf{N}_{1-4} + \mathbf{N}_{5-8} \\ -\mathbf{N}_{1-4} + \mathbf{N}_{5-8} \end{array} \right] = \left[\begin{array}{c} \mathbf{N}^m(\xi,\eta) \\ \zeta\mathbf{N}^m(\xi,\eta) \end{array} \right] \tag{20}$$

where $N_c^m = \frac{1}{4}(1 + \xi\xi_c)(1 + \eta\eta_c)$, $c = 1,\dots 4$. Note that unlike the transformed coordinates, the transformed shape functions do not exhibit the $1/2$ term which appears in (16) and (17). The Jacobian takes the form:

$$\mathbf{J}(\boldsymbol{\xi}) = \mathbf{X}\frac{\partial\mathbf{N}}{\partial\boldsymbol{\xi}^T} = \hat{\mathbf{X}}\mathbf{Q}\frac{\partial\mathbf{N}}{\partial\boldsymbol{\xi}^T} = [\mathbf{X}^m \ \Delta\mathbf{X}]\frac{\partial}{\partial\boldsymbol{\xi}^T} \left[\begin{array}{c} \mathbf{N}^m(\xi,\eta) \\ \zeta\mathbf{N}^m(\xi,\eta) \end{array} \right] =$$

$$= \left[(\mathbf{X}^m + \zeta\Delta\mathbf{X})\frac{\partial\mathbf{N}^m}{\partial\xi} \quad (\mathbf{X}^m + \zeta\Delta\mathbf{X})\frac{\partial\mathbf{N}^m}{\partial\eta} \quad \Delta\mathbf{X}\mathbf{N}^m \right] \tag{21}$$

Using Laplace's determinant expansion of a matrix, the determinant of $\mathbf{J}$ can be expressed in the form

$$\det[\mathbf{J}(\boldsymbol{\xi})] = J(\xi,\eta) + \zeta J^\zeta(\xi,\eta) + \zeta^2 J^{\zeta\zeta}(\xi,\eta) \tag{22}$$

where

$$J = \det\left[\mathbf{X}^m\frac{\partial\mathbf{N}^m}{\partial\xi} \ \mathbf{X}^m\frac{\partial\mathbf{N}^m}{\partial\eta} \ \Delta\mathbf{X}\mathbf{N}^m \right]$$

$$J^\zeta = \det\left[\mathbf{X}^m\frac{\partial\mathbf{N}^m}{\partial\xi} \ \Delta\mathbf{X}\frac{\partial\mathbf{N}^m}{\partial\eta} \ \Delta\mathbf{X}\mathbf{N}^m \right] + \det\left[\Delta\mathbf{X}\frac{\partial\mathbf{N}^m}{\partial\xi} \ \mathbf{X}^m\frac{\partial\mathbf{N}^m}{\partial\eta} \ \Delta\mathbf{X}\mathbf{N}^m \right] \tag{23}$$

$$J^{\zeta\zeta} = \det\left[\Delta\mathbf{X}\frac{\partial\mathbf{N}^m}{\partial\xi} \ \Delta\mathbf{X}\frac{\partial\mathbf{N}^m}{\partial\eta} \ \Delta\mathbf{X}\mathbf{N}^m \right]$$

Without loss of generality, $\det[\mathbf{J}(\boldsymbol{\xi})]$ will be assumed to be strictly positive in Ω^e, excluding in this way singular geometry transformations and orientation changes. Using the expression (22) of the Jacobian determinant, the element volume becomes

$$V = \int_{\boxdot} \det[\mathbf{J}(\boldsymbol{\xi})]d\xi d\eta d\zeta = \int_\square \left\{ \int_{-1}^1 \left[J(\xi,\eta) + \zeta J^\zeta(\xi,\eta) + \zeta^2 J^{\zeta\zeta}(\xi,\eta) \right] d\zeta \right\} d\xi d\eta =$$

$$= \int_\square \left[2J(\xi,\eta) + \frac{2}{3}J^{\zeta\zeta}(\xi,\eta) \right] d\xi d\eta \tag{24}$$

In the case of a parallelepiped distortion, it is easy to verify that both J^ζ and $J^{\zeta\zeta}$ vanish, J is constant and the element volume is completely determined by $J = V/8$, while, in the case of an arbitrary distortion, J^ζ and $J^{\zeta\zeta}$ are in general non-zero, even though they become smaller and smaller with respect to J as the thickness decreases.

It is also of interest to compute the area A of the element middle surface, defined as the surface at $\zeta = 0$. This is given by

$$A = \int_\square \left\| \frac{\partial\mathbf{x}}{\partial\xi} \times \frac{\partial\mathbf{x}}{\partial\eta} \right\|_{\zeta=0} d\xi d\eta = \int_\square j(\xi,\eta)d\xi d\eta \tag{25}$$

where $j(\xi,\eta)$ is the Jacobian of the surface transformation from the parent square to the distorted configuration.

2.2. Element equivalent nodal forces

Let $\mathbf{u}(\mathbf{x})$ denote the displacement field. According to the isoparametric paradigm, $\mathbf{u}(\mathbf{x})$ is interpolated over the element in terms of its nodal values $\underset{3\times 8}{\mathbf{U}}$ by the same shape functions used for the geometry, i.e. $\mathbf{u}(\mathbf{x}(\boldsymbol{\xi})) = \mathbf{U}\mathbf{N}(\boldsymbol{\xi})$. The matrix $\underset{3\times 8}{\mathbf{B}}(\mathbf{x}(\boldsymbol{\xi}))$ gathering the spatial gradients of nodal shape functions is defined as

$$\mathbf{B}(\mathbf{x}(\boldsymbol{\xi})) = \frac{\partial \mathbf{N}^T(\mathbf{x})}{\partial \mathbf{x}} = \mathbf{J}^{-T}(\boldsymbol{\xi})\frac{\partial \mathbf{N}^T(\boldsymbol{\xi})}{\partial \boldsymbol{\xi}} \tag{26}$$

Under the assumption of infinitesimal strains, the strain field over the element is defined by

$$\underset{3\times 3}{\boldsymbol{\varepsilon}}(\mathbf{x}) = \frac{1}{2}\left[\mathbf{U}\mathbf{B}^T(\mathbf{x}) + \mathbf{B}(\mathbf{x})\mathbf{U}^T\right] \tag{27}$$

Noting that, for an isotropic linear elastic material, the trace of $\boldsymbol{\varepsilon}$ can be expressed as

$$\mathbf{I}_3 : \boldsymbol{\varepsilon} = \frac{1}{2}\left[(\mathbf{I}_3\mathbf{B}) : \mathbf{U} + (\mathbf{B}^T\mathbf{I}_3) : \mathbf{U}^T\right] = \mathbf{B} : \mathbf{U} \tag{28}$$

the stress field is obtained as

$$\boldsymbol{\sigma} = \lambda(\mathbf{B} : \mathbf{U})\mathbf{I}_3 + \mu(\mathbf{U}\mathbf{B}^T + \mathbf{B}\mathbf{U}^T) \tag{29}$$

where λ and μ are Lame's constants.

The equivalent internal nodal forces $\underset{3\times 8}{\mathbf{F}}^{int}$ are obtained in the usual way considering a virtual displacement $\delta\mathbf{u}(\mathbf{x}) = \delta\mathbf{U}\mathbf{N}(\mathbf{x})$ and the corresponding virtual strains $\delta\boldsymbol{\varepsilon}(\mathbf{x})$:

$$\delta\mathbf{U} : \mathbf{F}^{int} = \int_{\Omega^e} \delta\boldsymbol{\varepsilon} : \boldsymbol{\sigma}\, d\Omega = \int_{\Omega^e} \delta\mathbf{U}\mathbf{B}^T : \boldsymbol{\sigma}\, d\Omega = \delta\mathbf{U} : \int_{\Omega^e} \boldsymbol{\sigma}\mathbf{B}\, d\Omega \quad \forall\delta\mathbf{U} \tag{30}$$

Defining as $\ddot{\mathbf{u}}(\mathbf{x}) = \ddot{\mathbf{U}}\mathbf{N}(\mathbf{x})$ the discretized acceleration field, the equivalent inertia nodal forces are similarly obtained as

$$-\delta\mathbf{U} : \mathbf{F}^i = \int_{\Omega^e} \rho\, \delta\mathbf{u}(\mathbf{x}) \cdot \ddot{\mathbf{u}}(\mathbf{x})\, d\Omega = \int_{\Omega^e} \rho(\delta\mathbf{U}\mathbf{N}(\mathbf{x})) \cdot (\ddot{\mathbf{U}}\mathbf{N}(\mathbf{x}))\, d\Omega$$

$$= \delta\mathbf{U} : \left[\ddot{\mathbf{U}} \int_{\Omega^e} \rho\mathbf{N}(\mathbf{x})\mathbf{N}^T(\mathbf{x})\, d\Omega\right] = \delta\mathbf{U} : \ddot{\mathbf{U}}\underset{8\times 8}{\mathbf{M}} \quad \forall\delta\mathbf{U} \tag{31}$$

The integral in (31) defines the consistent mass matrix $\mathbf{M}$. Its lumped version $\bar{\mathbf{M}}$, to be used in explicit dynamics applications, can be obtained using one of the several approaches available in the literature. The simplest lumping procedure, and the one which will be adopted in this work, consists of placing the row sum of the terms in $\mathbf{N}\mathbf{N}^T$ in (31) as diagonal entries and setting to zero the extra-diagonal terms (see e.g. [27]). Taking into account the partition of unity property of $\mathbf{N}$, this amounts to replace $\mathbf{N}\mathbf{N}^T$ by $\mathrm{diag}[\mathbf{N}_a \sum_{b=1}^{8} \mathbf{N}_b^T] = \mathrm{diag}[\mathbf{N}_a]$. This procedure guarantees the correct energy representation in translational rigid body motions, i.e., defining as $\underset{3\times 8}{\delta\mathbf{U}^{tr}} = \underset{3\times 1}{\delta\mathbf{u}^{tr}}\,\underset{1\times 8}{\mathbb{1}_8^T}$ the nodal displacements corresponding to a translational rigid body motion, with $\delta\mathbf{u}^{tr} = \mathrm{const}$ and $\mathbb{1}_8 = [1\ 1\ 1\ 1\ 1\ 1\ 1\ 1]^T$, one has:

$$-\delta\mathbf{U}^{tr} : \bar{\mathbf{F}}^i = \delta\mathbf{U}^{tr} : \left[\ddot{\mathbf{U}} \int_{\Omega^e} \rho\mathbf{N}(\mathbf{x})\mathbf{N}^T(\mathbf{x})\, d\Omega\right]$$

$$= \delta\mathbf{U}^{tr} : \left[\ddot{\mathbf{U}} \int_{\Omega^e} \rho\,\mathrm{diag}[N_a]\, d\Omega\right] \tag{32}$$

$$= \delta\mathbf{U}^{tr} : \ddot{\mathbf{U}}\bar{\mathbf{M}} \quad \forall\delta\mathbf{U}^{tr} = \delta\mathbf{u}^{tr}\,\mathbb{1}_8^T$$

where the bar superposed to $\mathbf{F}^i$ means that the inertia forces are obtained through a lumped mass matrix. This can be easily shown by noting that

$$\delta\mathbf{U}^{tr} : \left[\ddot{\mathbf{U}} \int_{\Omega^e} \rho \mathbf{N}(\mathbf{x})\mathbf{N}^T(\mathbf{x}) \, d\Omega\right] = \delta\mathbf{u}^{tr} \cdot \left[\ddot{\mathbf{U}} \int_{\Omega^e} \rho \mathbf{N}\mathbf{N}^T \mathbb{1}_8 \, d\Omega\right] \quad \forall \delta\mathbf{u}^{tr} \tag{33}$$

Since $\mathbf{N}^T \mathbb{1}_8 = 1$ and $\mathbf{N} = \text{diag}[N_a]\mathbb{1}_8$, one finally obtains (32). Other lumping techniques, such as the HRZ [29], can be also considered in combination with the proposed mass scaling technique, without substantial modifications of the conceptual approach.

2.3. Degrees of freedom transformation and selective mass scaling

The same linear transformation used in (16) and (17) for nodal coordinates is used for nodal displacements

$$\hat{\mathbf{U}}_{3\times 8} = \left[\underset{3\times 4}{\mathbf{U}^m} \ \underset{3\times 4}{\Delta\mathbf{U}}\right] = \mathbf{U}\mathbf{Q}^{-1}, \quad \mathbf{U} = \hat{\mathbf{U}}\mathbf{Q} \tag{34}$$

Applying the linear transformation (34), the internal nodal forces $\mathbf{F}^{int}$ in (30) are transformed accordingly as

$$\delta\mathbf{U} : \mathbf{F}^{int} = \delta\hat{\mathbf{U}} : \hat{\mathbf{F}}^{int} = \delta\hat{\mathbf{U}} : \int_{\Omega^e} \left[\lambda(\hat{\mathbf{U}} : \hat{\mathbf{B}})\hat{\mathbf{B}} + \mu(\hat{\mathbf{U}}\hat{\mathbf{B}}^T + \hat{\mathbf{B}}\hat{\mathbf{U}}^T)\hat{\mathbf{B}}\right] d\Omega \quad \forall\delta\hat{\mathbf{U}} \tag{35}$$

where

$$\hat{\mathbf{F}}^{int} = \mathbf{F}^{int}\mathbf{Q}^T, \quad \hat{\mathbf{B}} = \mathbf{J}^{-T} \left[\frac{\partial(\mathbf{N}^m)^T}{\partial\boldsymbol{\xi}} \ \frac{\partial(\zeta\mathbf{N}^m)^T}{\partial\boldsymbol{\xi}}\right] = \mathbf{B}\mathbf{Q}^T \tag{36}$$

The inertia nodal forces $\bar{\mathbf{F}}^i$ are transformed in a similar way:

$$-\delta\mathbf{U} : \bar{\mathbf{F}}^i = -\delta\hat{\mathbf{U}} : \hat{\bar{\mathbf{F}}}^i = \delta\hat{\mathbf{U}} : \left[\ddot{\hat{\mathbf{U}}} \int_{\Omega^e} \rho \, \mathbf{Q} \, \text{diag}[N_a(\mathbf{x})]\mathbf{Q}^T \, d\Omega\right] \quad \forall\delta\hat{\mathbf{U}}, \quad a = 1, \ldots 8 \tag{37}$$

with

$$\hat{\bar{\mathbf{F}}}^i = \bar{\mathbf{F}}^i\mathbf{Q}^T, \quad \ddot{\hat{\mathbf{U}}} = \ddot{\mathbf{U}}\mathbf{Q}^{-1} \tag{38}$$

Taking into account the expression (18) of $\mathbf{Q}$ and (22) of $\det[\mathbf{J}]$, assuming that $\rho = \rho(\xi, \eta)$ and recalling from (20) that $\mathbf{N}_{1-4} + \mathbf{N}_{5-8} = \mathbf{N}^m$, $-\mathbf{N}_{1-4} + \mathbf{N}_{5-8} = \zeta\mathbf{N}^m$, the inertia forces $\hat{\bar{\mathbf{F}}}^i$ in (37) can be written as

$$\begin{aligned}
-\hat{\bar{\mathbf{F}}}^i &= \ddot{\hat{\mathbf{U}}} \int_{\square} \rho \left\{\int_{-1}^{1} \begin{bmatrix} \text{diag}[N_c^m] & \zeta\text{diag}[N_c^m] \\ \zeta\text{diag}[N_c^m] & \zeta^2\text{diag}[N_c^m] \end{bmatrix} \left(J + \zeta J^\zeta + \zeta^2 J^{\zeta\zeta}\right) d\zeta\right\} d\xi d\eta \\
&= \ddot{\hat{\mathbf{U}}} \int_{\square} 2\rho \begin{bmatrix} \left(J + \frac{J^{\zeta\zeta}}{3}\right)\text{diag}[N_c^m] & \frac{J^\zeta}{3}\text{diag}[N_c^m] \\ \frac{J^\zeta}{3}\text{diag}[N_c^m] & \left(J + \frac{J^{\zeta\zeta}}{3}\right)\text{diag}[N_c^m] \end{bmatrix} d\xi d\eta = \ddot{\hat{\mathbf{U}}}\hat{\mathbf{M}}
\end{aligned} \tag{39}$$

where subscript $c = 1, \ldots 4$ runs over the four middle surface element corners.

The mass matrix $\underset{8\times 8}{\hat{\mathbf{M}}}$ in (39) is not diagonal. As already noted, for a parallelepiped element $J^\zeta = J^{\zeta\zeta} = 0$ and the extra-diagonal blocks disappear. For solid-shell type distortions, where the thickness is small compared to the in-plane dimensions, the extra-diagonal terms are small compared to the diagonal ones and can be neglected, obtaining again a diagonal mass matrix:

$$-\hat{\bar{\bar{\mathbf{F}}}}^i = \ddot{\hat{\mathbf{U}}} \int_{\square} 2\rho \left(J + \frac{J^{\zeta\zeta}}{3}\right) \begin{bmatrix} \text{diag}[N_c^m] & \mathbf{0} \\ \mathbf{0} & \text{diag}[N_c^m] \end{bmatrix} d\xi d\eta = \ddot{\hat{\mathbf{U}}}\hat{\bar{\mathbf{M}}} \tag{40}$$

The second bar over $\hat{\bar{\mathbf{F}}}^i$ and $\hat{\bar{\mathbf{M}}}$ in (40) means that the extra-diagonal terms of the transformed lumped mass matrix have been discarded.

Neglecting extra-diagonal terms does not compromise the correct representation of energy for translational rigid body motions, even though it implies slight modifications of the element spectrum, if compared to the original element with lumped mass matrix. The modification on the squares of the highest and lowest eigenfrequencies can be bounded using the Rayleigh quotient.

Let $\bar{\omega}_{max}^2$ and $\bar{\bar{\omega}}_{max}^2$ be the maximum eigenvalues with lumped $\bar{\mathbf{M}}$ (or equivalently $\hat{\bar{\mathbf{M}}}$, since the linear dofs transformation (34) does not alter the element spectrum) and with lumped-diagonalized $\hat{\bar{\bar{\mathbf{M}}}}$ mass matrices, respectively, and let $\hat{\bar{\mathbf{V}}}$ and $\hat{\bar{\bar{\mathbf{V}}}}$ be the corresponding eigenvectors. The eigenvalues can be expressed as

$$\bar{\omega}_{max}^2 = \frac{\hat{\bar{\mathbf{V}}} : \hat{\mathbf{F}}^{int}(\hat{\bar{\mathbf{V}}})}{\hat{\bar{\mathbf{V}}} : \hat{\bar{\mathbf{F}}}^i(\hat{\bar{\mathbf{V}}})}, \quad \bar{\bar{\omega}}_{max}^2 = \frac{\hat{\bar{\bar{\mathbf{V}}}} : \hat{\mathbf{F}}^{int}(\hat{\bar{\bar{\mathbf{V}}}})}{\hat{\bar{\bar{\mathbf{V}}}} : \hat{\bar{\bar{\mathbf{F}}}}^i(\hat{\bar{\bar{\mathbf{V}}}})} \tag{41}$$

Using the extremal property of Rayleigh quotient, one has that

$$\bar{\bar{\omega}}_{max}^2 \geq \frac{\hat{\bar{\mathbf{V}}} : \hat{\mathbf{F}}^{int}(\hat{\bar{\mathbf{V}}})}{\hat{\bar{\mathbf{V}}} : \hat{\bar{\bar{\mathbf{F}}}}^i(\hat{\bar{\mathbf{V}}})} = \bar{\omega}_{max}^2 \frac{\hat{\bar{\mathbf{V}}} : \hat{\bar{\mathbf{F}}}^i(\hat{\bar{\mathbf{V}}})}{\hat{\bar{\mathbf{V}}} : \hat{\bar{\bar{\mathbf{F}}}}^i(\hat{\bar{\mathbf{V}}})}$$

$$\bar{\omega}_{max}^2 \geq \frac{\hat{\bar{\bar{\mathbf{V}}}} : \hat{\mathbf{F}}^{int}(\hat{\bar{\bar{\mathbf{V}}}})}{\hat{\bar{\bar{\mathbf{V}}}} : \hat{\bar{\mathbf{F}}}^i(\hat{\bar{\bar{\mathbf{V}}}})} = \bar{\bar{\omega}}_{max}^2 \frac{\hat{\bar{\bar{\mathbf{V}}}} : \hat{\bar{\bar{\mathbf{F}}}}^i(\hat{\bar{\bar{\mathbf{V}}}})}{\hat{\bar{\bar{\mathbf{V}}}} : \hat{\bar{\mathbf{F}}}^i(\hat{\bar{\bar{\mathbf{V}}}})} \tag{42}$$

Taking into account that the two mass matrices have the same diagonal entries, using these inequalities the relative difference between the two eigenvalues can be bounded as follows

$$-2\frac{\bar{\bar{\mathbf{V}}}^m : \mathbf{F}^{i\,m}(\Delta\bar{\bar{\mathbf{V}}})}{\hat{\bar{\bar{\mathbf{V}}}} : \hat{\bar{\mathbf{F}}}^i(\hat{\bar{\bar{\mathbf{V}}}})} \leq \frac{\bar{\omega}_{max}^2 - \bar{\bar{\omega}}_{max}^2}{\bar{\omega}_{max}^2} \leq -2\frac{\bar{\mathbf{V}}^m : \mathbf{F}^{i\,m}(\Delta\bar{\mathbf{V}})}{\hat{\bar{\mathbf{V}}} : \hat{\bar{\bar{\mathbf{F}}}}^i(\hat{\bar{\mathbf{V}}})} \tag{43}$$

with

$$\hat{\mathbf{V}} = [\mathbf{V}^m \ \Delta\mathbf{V}], \quad \hat{\mathbf{F}}^i = [\mathbf{F}^{i\,m} \ \Delta\mathbf{F}^i]$$

$$\mathbf{V}^m : \mathbf{F}^{i\,m}(\Delta\mathbf{V}) = \mathbf{V}^m : \Delta\mathbf{V} \int_\square \frac{2}{3} J^\zeta \rho \,\mathrm{diag}[N_c^m] d\xi d\eta \quad c = 1, \dots 4 \tag{44}$$

Excluding the eigenvectors associated to zero eigenvalues and following the same path of reasoning as above, a similar delimitation can also be constructed for the element minimum eigenvalues. These bounds turn out to be very tight and the gap rapidly decreases with the thickness, as it can be verified by means of the following numerical investigation.

Let Ω^{p2}, Ω^{p5}, Ω^{p10} be three parallelepiped 8-node elements with in-plane dimensions equal to 5 mm and with thicknesses equal to $\frac{5}{2}$, $\frac{5}{5}$, $\frac{5}{10}$ mm, respectively. Let $\hat{\mathbf{X}}^{p2}$, $\hat{\mathbf{X}}^{p5}$, $\hat{\mathbf{X}}^{p10}$ be the matrices of the 24 transformed nodal coordinates of each element, expressed with respect to the element centroid. For each thickness, a population of 10000 coordinates perturbation matrices $\underset{3\times4}{\mathbf{d}^r}$ and $\underset{3\times4}{\Delta\mathbf{d}_{1-4}^r}$, $\underset{3\times4}{\Delta\mathbf{d}_{5-8}^r}$, $r = 2, 5, 10$ has been randomly generated. While $-1/2\,\mathbf{X}^{m\,p} \leq \mathbf{d}^r \leq 1/2\,\mathbf{X}^{m\,p}$ has been set, $\Delta\mathbf{d}_{1-4}^r$ and $\Delta\mathbf{d}_{5-8}^r$ have been constructed each one gathering as columns four of the randomly generated vectors $-h^r/4\,\mathbb{1}_3 \leq \Delta\mathbf{d}_a \leq h^r/4\,\mathbb{1}_3$, $a = 1, \dots 8$, where $h^r = 5/r$ is the reference parallelepiped thickness and $\mathbb{1}_3 = [1\ 1\ 1]^T$. As a result, 10000 randomly distorted elements of coordinates $\mathbf{X}_{1-4}^{p\,r} = (\mathbf{X}^{m\,p} + \mathbf{d}^r) - (\Delta\mathbf{X}^{p\,r} + \Delta\mathbf{d}_{1-4}^r)$, $\mathbf{X}_{5-8}^{p\,r} = (\mathbf{X}^{m\,p} + \mathbf{d}^r) + (\Delta\mathbf{X}^{p\,r} + \Delta\mathbf{d}_{5-8}^r)$ for each thickness. It is easy to verify that combinations of extreme values of these perturbations lead to significantly distorted elements, such as the one of the type $p2$ shown in Figure 2. The element coordinates are reported in Table I. For each element, the contributions of J^ζ, $J^{\zeta\zeta}$ and J to the element volume have been computed numerically using a $5 \times 5 \times 5$ Gauss point integration and the complete spectrum has been computed, considering the following material properties: $E = 1768$ MPa, $\nu = 0.3$, $\rho = 3 \cdot 10^3$ kg/m³. The maximum values, among the three populations of 10000 elements each, of the ratio J^ζ/J and of the differences between the maximum and minimum eigenvalues obtained with the original lumped mass matrix $\bar{\mathbf{M}}$ and with the diagonalized one, $\hat{\bar{\bar{\mathbf{M}}}}$, are summarized in Table II.

node:	1	2	3	4	5	6	7	8
x_1	-2.5401	1.9654	3.9992	-0.9892	-2.7658	0.7515	3.1159	-1.7921
x_2	-3.4673	-2.0530	2.3185	1.7620	-3.6264	-2.0002	2.2406	2.0127
x_3	-0.7060	-0.6628	-1.4059	-0.6439	0.7776	1.5762	1.3492	1.4014

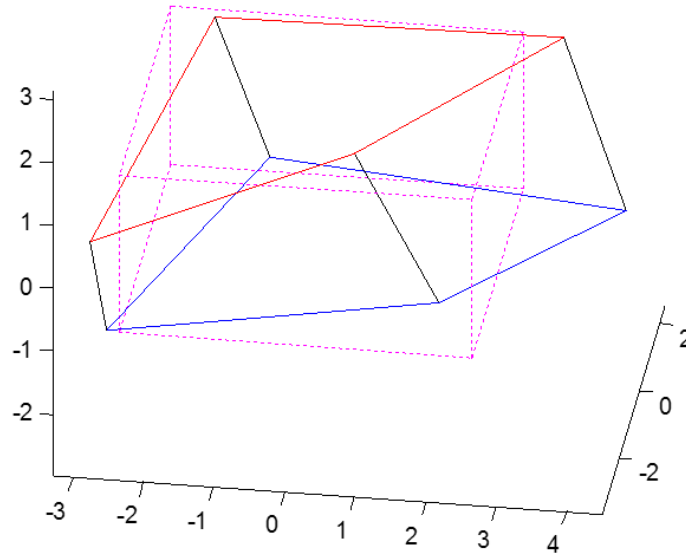Table I. Nodal coordinates of distorted element of family $p2$ in Figure 2.

Figure 2. Distorted solid-shell element of $p2$ family (i.e. thickness equal one half of the in-plane dimensions).

	$\max \left| J^\zeta / J \right|$	$\max \left| \frac{\bar{\omega}^2_{min} - \bar{\bar{\omega}}^2_{min}}{\bar{\omega}^2_{min}} \right|$	$\max \left| \frac{\bar{\omega}^2_{max} - \bar{\bar{\omega}}^2_{max}}{\bar{\omega}^2_{max}} \right|$
$p2$	0.3021	0.0460	0.0269
$p5$	0.1173	0.0114	0.0021
$p10$	0.0639	0.0024	0.0002

Table II. Comparison between max and min element eigenvalues using $\bar{\mathbf{M}}$ and $\hat{\bar{\mathbf{M}}}$ within considered population of randomly distorted 3×10000 elements.

In conclusion, the diagonalization of the the transformed lumped mass matrix $\hat{\bar{\mathbf{M}}}$ produces only negligible variations of the element spectrum, much smaller than those implied, e.g., by the initial mass lumping with respect to the original consistent mass matrix. Since the eigenfrequencies are the square roots of the eigenvalues, the variations on the eigenfrequencies turn out to be about one half of what is reported in Table II. In view of this result, the diagonal mass matrix $\hat{\bar{\mathbf{M}}}$ will be used henceforth and the double bar over the symbol ω will be omitted to simplify the notation.

In [20], it has been shown how the element maximum eigenfrequency can be scaled down by selectively multiplying some entries of $\hat{\bar{\mathbf{M}}}$ by a scaling factor $\alpha > 1$, leading to modified nodal

equivalent, selectively scaled inertia forces $(\bar{\hat{\bar{\mathbf{F}}}}^i)^\alpha$

$$-(\bar{\hat{\bar{\mathbf{F}}}}^i)^\alpha = -\bar{\hat{\bar{\mathbf{F}}}}^i\mathbf{I}_8^\alpha = \ddot{\hat{\mathbf{U}}}\int_\square 2\rho\left(J + \frac{2}{3}J^{\zeta\zeta}\right)\left[\begin{array}{cc} \text{diag}[N_c^m] & \mathbf{0} \\ \mathbf{0} & \alpha\text{diag}[N_c^m] \end{array}\right]d\xi d\eta = \ddot{\hat{\mathbf{U}}}\bar{\hat{\bar{\mathbf{M}}}}^\alpha \quad (45)$$

where $\mathbf{I}_8^\alpha$ is defined as

$$\mathbf{I}_8^\alpha = \left[\begin{array}{cc} \mathbf{I}_4 & \mathbf{0} \\ \mathbf{0} & \alpha\mathbf{I}_4 \end{array}\right] \quad (46)$$

The same type of selective mass scaling will be adopted also in the present paper. However, in [20] only parallelepiped elements were considered. In the present work, the proposed selective mass scaling will be applied to arbitrarily distorted solid-shell elements. As it will be discussed in the next section, to obtain an analytical estimate of the scaled element maximum eigenfrequency, as in [26] use will be made of a one Gauss point integration rule (constant strain element).

2.4. Equivalence between mass scaling and geometric scaling

An interesting interpretation of the selective mass scaling in (45) can be obtained by transferring the scaling from the inertia forces to the internal forces. Starting from the variational form of the equation of motion (in the simple case of free motion)

$$\delta\hat{\mathbf{U}} : \left(\ddot{\hat{\mathbf{U}}}\hat{\mathbf{M}}^\alpha + \hat{\mathbf{F}}^{int}\right) = \mathbf{0} \quad \forall\delta\hat{\mathbf{U}} \quad (47)$$

one can rewrite the virtual work of the inertia forces as

$$\delta\hat{\mathbf{U}} : \ddot{\hat{\mathbf{U}}}\hat{\mathbf{M}}^\alpha = \delta\hat{\mathbf{U}} : \ddot{\hat{\mathbf{U}}}\mathbf{I}_8^{\sqrt{\alpha}}\hat{\mathbf{M}}\mathbf{I}_8^{\sqrt{\alpha}} = \left(\delta\hat{\mathbf{U}}\,\mathbf{I}_8^{\sqrt{\alpha}}\right) : \left(\ddot{\hat{\mathbf{U}}}\mathbf{I}_8^{\sqrt{\alpha}}\right)\hat{\mathbf{M}} = \delta\hat{\mathbf{U}}^{\sqrt{\alpha}} : \ddot{\hat{\mathbf{U}}}^{\sqrt{\alpha}}\hat{\mathbf{M}} \quad (48)$$

where the following definitions have been used

$$\mathbf{I}_8^{\sqrt{\alpha}} = \left[\begin{array}{cc} \mathbf{I}_4 & \mathbf{0} \\ \mathbf{0} & \sqrt{\alpha}\mathbf{I}_4 \end{array}\right], \quad \delta\hat{\mathbf{U}}^{\sqrt{\alpha}} = \left[\begin{array}{cc} \delta\mathbf{U}^m & \sqrt{\alpha}\,\delta\Delta\mathbf{U} \end{array}\right], \quad \ddot{\hat{\mathbf{U}}}^{\sqrt{\alpha}} = \left[\begin{array}{cc} \ddot{\mathbf{U}}^m & \sqrt{\alpha}\Delta\ddot{\mathbf{U}} \end{array}\right] \quad (49)$$

The virtual work of the internal forces is modified accordingly

$$\delta\hat{\mathbf{U}} : \hat{\mathbf{F}}^{int} = \delta\hat{\mathbf{U}}^{\sqrt{\alpha}} : \left(\hat{\mathbf{F}}^{int}\right)^{1/\sqrt{\alpha}} \quad (50)$$

where $\left(\hat{\mathbf{F}}^{int}\right)^{1/\sqrt{\alpha}} = \hat{\mathbf{F}}^{int}\mathbf{I}_8^{1/\sqrt{\alpha}}$, with obvious definition of $\mathbf{I}_8^{1/\sqrt{\alpha}}$. Notice that the symbols α, $\sqrt{\alpha}$ and $1/\sqrt{\alpha}$ in superscript position are not to be intended as exponents, but as qualifiers of the scaling implemented on the corresponding array or matrix. Taking into account the expression (35) of $\hat{\mathbf{F}}^{int}$ and defining $\hat{\mathbf{B}}^{1/\sqrt{\alpha}} = \hat{\mathbf{B}}\mathbf{I}_8^{1/\sqrt{\alpha}}$, $\hat{\mathbf{U}}^{\sqrt{\alpha}} = \hat{\mathbf{U}}\mathbf{I}_8^{\sqrt{\alpha}}$, one finally obtains

$$\delta\hat{\mathbf{U}} : \hat{\mathbf{F}}^{int} = \delta\hat{\mathbf{U}}^{\sqrt{\alpha}} : \int_{\Omega^e}\left[\lambda\left(\hat{\mathbf{U}}^{\sqrt{\alpha}} : \hat{\mathbf{B}}^{1/\sqrt{\alpha}}\right)\mathbf{I}_3 + \mu\left(\hat{\mathbf{U}}^{\sqrt{\alpha}}\left(\hat{\mathbf{B}}^{1/\sqrt{\alpha}}\right)^T + \hat{\mathbf{B}}^{1/\sqrt{\alpha}}\left(\hat{\mathbf{U}}^{\sqrt{\alpha}}\right)^T\right)\right]\hat{\mathbf{B}}^{1/\sqrt{\alpha}}\,d\Omega$$
$$= \delta\hat{\mathbf{U}}^{\sqrt{\alpha}} : \left(\hat{\mathbf{F}}^{int}\right)^{1/\sqrt{\alpha}}$$

$$(51)$$

The problems (47) and

$$\delta\hat{\mathbf{U}}^{\sqrt{\alpha}} : \left[\ddot{\hat{\mathbf{U}}}^{\sqrt{\alpha}}\hat{\mathbf{M}} + \left(\hat{\mathbf{F}}^{int}\right)^{1/\sqrt{\alpha}}\right] = \mathbf{0} \quad \forall\delta\hat{\mathbf{U}}^{\sqrt{\alpha}} \quad (52)$$

have the same eigenvalues, whereas the eigenvectors are scaled in a different way. In the latter problem, accelerations and displacements are selectively scaled while the mass matrix is not, so that the internal forces are scaled through a modification of the compatibility matrix $\hat{\mathbf{B}}$. In qualitative terms, the modification of $\hat{\mathbf{B}}$ can be interpreted as an enlargement of the element in the thickness
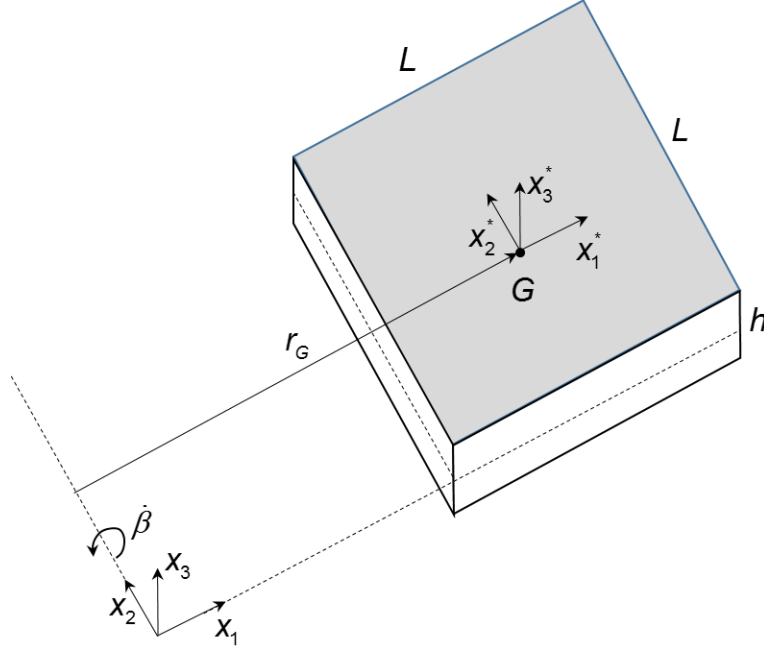
Figure 3. Test element used for assessment of rotational error.

direction (smaller strains would be obtained for the same relative displacement). The equivalence between selective mass and geometric scalings will be proved in more rigorous terms in the next Section, in the case of reduced one-Gauss point integration.

The possibility to improve the stiffness matrix conditioning (or equivalently to reduce higher eigenfrequencies) by artificially increasing the element thickness has been investigated by several authors (see e.g. [22, 23, 24]), while in [21] Olovsson et al. proposed a direct scaling of accelerations, leaving the mass matrix unaltered.

2.5. Error due to scaled rotational inertia

While the selective mass scaling proposed in (45) does not affect translational rigid body motions, it does affect rigid body rotations. To asses this effect, the roto-translational motion of the parallelepiped element of constant density ρ in Figure 3 is analyzed.

The element has a square $L \times L$ basis and thickness h. For convenience, the element sides in the initial configuration are taken aligned with the axes of the global reference system. G is the element centroid of coordinates $\mathbf{X}_G$, which is at a distance r_G from the x_2 axis, which is assumed to be the rotation axis.

A rotation with constant angular velocity $\dot{\beta}$ is considered. Rigid body rotations around x_2 are defined by the rotation matrix $\mathbf{R}$

$$\mathbf{R} = \begin{bmatrix} \cos\beta & 0 & -\sin\beta \\ 0 & 1 & 0 \\ \sin\beta & 0 & \cos\beta \end{bmatrix} \tag{53}$$

so that the displaced configuration and velocity field are obtained as

$$\mathbf{x} = \mathbf{R}\mathbf{x}_0, \quad \dot{\mathbf{u}} = \dot{\mathbf{R}}\mathbf{x}_0 \tag{54}$$

where $\mathbf{x}_0$ denotes coordinates in the original configuration and

$$\dot{\mathbf{R}} = \dot{\beta} \begin{bmatrix} -\sin\beta & 0 & -\cos\beta \\ 0 & 0 & 0 \\ \cos\beta & 0 & -\sin\beta \end{bmatrix}, \quad \dot{\mathbf{R}}^T\mathbf{R} = \dot{\beta} \begin{bmatrix} 1 & 0 & 0 \\ 0 & 0 & 0 \\ 0 & 0 & 1 \end{bmatrix} \tag{55}$$

It is convenient to adopt a reference system placed in the element centroid, such that

$$\mathbf{x}_0 = \mathbf{X}_G + \mathbf{x}_0^\star, \quad \dot{\mathbf{u}} = \dot{\mathbf{R}}(\mathbf{X}_G + \mathbf{x}_0^\star) \tag{56}$$

where $\mathbf{x}_0^\star$ are coordinates measured with respect to the centroid.

The element kinetic energy is given by

$$K = \frac{1}{2} \int_{\Omega^e} \rho \dot{\mathbf{u}}^T \dot{\mathbf{u}} \, d\Omega = \frac{1}{2} \int_{\Omega^e} \rho \left(\mathbf{X}_G^T + \mathbf{x}_0^{\star T} \right) \dot{\mathbf{R}} \mathbf{R} (\mathbf{X}_G + \mathbf{x}_0^\star) d\Omega \tag{57}$$

Noting that

$$\int_{\Omega^e} \mathbf{x}_0^{\star T} \dot{\mathbf{R}} \mathbf{R} \mathbf{X}_G d\Omega = 0$$
$$\int_{\Omega^e} \mathbf{X}_G^T \dot{\mathbf{R}} \mathbf{R} \mathbf{X}_G d\Omega = \dot{\beta} V_0 r_G^2 \tag{58}$$
$$\int_{\Omega^e} \mathbf{x}_0^{\star T} \dot{\mathbf{R}} \mathbf{R} \mathbf{x}_0^\star d\Omega = \dot{\beta} V_0 \frac{1}{12}(L^2 + h^2)$$

$V_0 = L^2 h$ being the element volume, one obtains

$$K = \frac{1}{2} \dot{\beta} \rho V_0 \left[r_G^2 + \frac{1}{12}(L^2 + h^2) \right] \tag{59}$$

By setting

$$L = \frac{2}{\gamma_1} = \frac{2}{\gamma_2}, \quad h = \frac{2}{\gamma_3} = \frac{\gamma_1}{\gamma_3} L = \frac{\gamma_2}{\gamma_3} L \tag{60}$$

$\gamma_1 = \gamma_2$ and γ_3 being the eigenvalues in (15), and defining $\gamma = \gamma_3/\gamma_1 = \gamma_3/\gamma_2$, one can write

$$K = \frac{1}{2} \dot{\beta} \rho V_0 \left[r_G^2 + \frac{L^2}{12}(1 + \frac{1}{\gamma^2}) \right] \tag{61}$$

The discretized velocity field is expressed as

$$\dot{\mathbf{u}} = \dot{\mathbf{U}} \mathbf{N}(\boldsymbol{\xi}) = \dot{\mathbf{R}} \left(\underset{3 \times 1}{\mathbf{X}_G} \mathbb{1}_8^T + \underset{3 \times 8}{\mathbf{X}_0^\star} \right) \mathbf{N}(\boldsymbol{\xi}) \tag{62}$$

where $\mathbf{X}_0^\star$ is the matrix of nodal coordinates in the element local reference system. According to (18), the transformed nodal velocities are given by

$$\dot{\hat{\mathbf{U}}} = \frac{1}{2} \dot{\mathbf{U}} \mathbf{Q}^T = \frac{1}{2} \dot{\mathbf{R}} (\hat{\mathbf{X}}_G + \hat{\mathbf{X}}_0^\star) \tag{63}$$

with

$$\underset{3 \times 8}{\hat{\mathbf{X}}_G} = \frac{1}{2} \underset{3 \times 1}{\mathbf{X}_G} \underset{1 \times 8}{\mathbb{1}_8^T} \underset{8 \times 8}{\mathbf{Q}^T} = \mathbf{X}_G [2\ 2\ 2\ 2\ 0\ 0\ 0\ 0], \quad \hat{\mathbf{X}}_0^\star = \frac{1}{2} \mathbf{X}_0^\star \mathbf{Q}^T \tag{64}$$

Using the definition of the transformed lumped mass matrix in (40) and considering that the element is a parallelepiped, one has $\bar{\bar{\mathbf{M}}} = 2\rho J \mathbf{I}_8$ where $8J = V_0$ is the element volume. The discretized kinetic energy is then given by

$$\bar{\bar{K}} = \frac{1}{2} \dot{\hat{\mathbf{U}}} : \dot{\hat{\mathbf{U}}} \bar{\bar{\mathbf{M}}} = \frac{1}{2} \dot{\hat{\mathbf{U}}} : \dot{\hat{\mathbf{U}}} (2\rho J \mathbf{I}_8) \tag{65}$$

Assuming the rotational motion in (54), substituting (63) in (65) and taking into account that

$$(\dot{\mathbf{R}} \hat{\mathbf{X}}_G) : (\dot{\mathbf{R}} \hat{\mathbf{X}}_G) = 4\dot{\beta}^2 r_G^2$$
$$(\dot{\mathbf{R}} \hat{\mathbf{X}}_G) : (\dot{\mathbf{R}} \hat{\mathbf{X}}_0^\star) = 0 \tag{66}$$
$$(\dot{\mathbf{R}} \hat{\mathbf{X}}^\star) : (\dot{\mathbf{R}} \hat{\mathbf{X}}_0^\star) = \dot{\beta}^2 (L^2 + h^2)$$

one obtains

$$\dot{\bar{\bar{K}}} = \frac{1}{2}2\rho J\left[\dot{\mathbf{R}}(\hat{\mathbf{X}}_G + \hat{\mathbf{X}}_0^\star)\right] : \left[\dot{\mathbf{R}}(\hat{\mathbf{X}}_G + \hat{\mathbf{X}}_0^\star)\mathbf{I}_8\right] = \frac{1}{2}\dot{\beta}\rho V_0\left[r_G^2 + \frac{1}{4}(L^2 + h^2)\right] \qquad (67)$$

For the considered parallelepiped, the scaled transformed lumped mass matrix (45) is given by $\bar{\bar{\mathbf{M}}}^\alpha = 2\rho J\mathbf{I}_8^\alpha$ with the corresponding expression of the scaled kinetic energy

$$\dot{\bar{\bar{K}}}^\alpha = \frac{1}{2}2\rho J\left[\dot{\mathbf{R}}(\hat{\mathbf{X}}_G + \hat{\mathbf{X}}_0^\star)\right] : \left[\dot{\mathbf{R}}(\hat{\mathbf{X}}_G + \hat{\mathbf{X}}_0^\star)\mathbf{I}_8^\alpha\right] = \frac{1}{2}\dot{\beta}\rho V_0\left[r_G^2 + \frac{1}{4}(L^2 + \alpha h^2)\right] \qquad (68)$$

As expected, the adopted selective mass scaling leads to an alteration of the kinetic energy associated to a rotational motion. The relative error with respect to the non-scaled energy is given by

$$e = \frac{\dot{\bar{\bar{K}}}^\alpha - \dot{\bar{\bar{K}}}}{\dot{\bar{\bar{K}}}} = (\alpha - 1)\frac{h^2}{4r_G^2 + L^2 + h^2} \qquad (69)$$

Making use of the relation $h = L/\gamma$, the error can be rewritten as

$$e = (\alpha - 1)\frac{1}{\gamma^2\left[4\frac{r_G^2}{L^2} + \left(1 + \frac{1}{\gamma^2}\right)\right]} \qquad (70)$$

For a pure rotational motion, one has $r_G = 0$, and for thin shells ($\gamma \ggg 1$) the error is simply given by

$$e = (\alpha - 1)\frac{1}{\gamma^2\left(1 + \frac{1}{\gamma^2}\right)} \approx (\alpha - 1)\frac{1}{\gamma^2} \qquad (71)$$

and therefore it depends linearly on the mass scaling and quadratically on the element thickness to width ratio $1/\gamma$ (note that $1/\gamma$ increases for increasing thickness).

If $r_G > 0$, the motion is roto-translational. The term $(r_G/L)^2$ measures the relative weight of the translational contribution to the kinetic energy with respect to the rotational one. For thin shells ($\gamma \ggg 1$) and r_G/L sufficiently large, a good estimate $\bar{e}$ of the energy error implied by the proposed selective mass scaling is given by

$$\bar{e} \approx (\alpha - 1)\frac{1}{4\gamma^2\left(\frac{r_g}{L}\right)^2} \qquad (72)$$

and is negligible in most cases, as it will be shown in the numerical examples. However, it has to be taken into account in all those cases where the motion contains a prevailing large rotational component.

3. COMPUTATION OF ELEMENT MAXIMUM EIGENFREQUENCY

3.1. Reduced integration solid-shell elements

After selective mass scaling has been applied, one remains with the problem of computing the critical time step size which, according to (2), can be estimated from the maximum element eigenfrequency. In the case of distorted hexahedrical elements, an effective estimate was proposed by Flanagan and Belytschko in [26], based on a constant strain (one Gauss point) approximation. Clearly, reduced integration elements have a maximum eigenfrequency which is not equal to their fully integrated counterparts. The difference can be quantitatively assessed by a numerical investigation of the type considered in Section 2.3, based on a population of 3×10000 randomly distorted elements. For each element , the eigenfrequency $\omega_{max(1\times1\times1)}$, obtained using a one Gauss point reduced integration and lumped mass matrices, has been compared with the corresponding

	max $\dfrac{\omega_{\max(1\times1\times1)}-\omega_{\max(5\times5\times5)}}{\omega_{\max(5\times5\times5)}}$	max $\dfrac{\omega_{\max(1\times1\times1)}-\omega_{\max(1\times1\times5)}}{\omega_{\max(1\times1\times5)}}$
$p2$	0.0910	0.0050
$p5$	0.0891	0.0006
$p10$	0.1023	0.0001

Table III. Comparison between max eigenfrequencies: $\omega_{\max(1\times1\times1)} \rightarrow$ reduced integration rule for uniform strain elements; $\omega_{\max(1\times1\times5)} \rightarrow$ reduced integration rule for solid-shell elements; $\omega_{\max(5\times5\times5)} \rightarrow$ full integration rule.

eigenfrequency obtained with a $5 \times 5 \times 5$ Gauss integration rule. The maximum difference, defined as $\max\{(\omega_{\max(1\times1\times1)} - \omega_{\max(5\times5\times5)})/\omega_{\max(5\times5\times5)}\}$, is about 10%, tending to decrease with the thickness to in-plane dimension ratio. The sign of the difference is almost always negative, as it is expected, since the one Gauss point element is in general less stiff than the fully integrated element.

When solid-shell elements are used in explicit dynamics analyses, a reduced integration rule with one Gauss point in the in-plane direction and at least two Gauss points in the thickness direction is often used to reduce the computational burden and, at the same time, to provide an accurate description of the element bending behavior. The accuracy of the uniform strain element estimate has been numerically assessed also in this case, using the same population of 3×10000 distorted elements, and comparing $\omega_{\max(1\times1\times1)}$ with the maximum eigenfrequency obtained using a $(1 \times 1 \times 5)$ integration rule, i.e. one Gauss point in the in-plane direction and 5 Gauss points through the thickness. In this case, the maximum difference defined as $\max\{(\omega_{\max(1\times1\times1)} - \omega_{\max(1\times1\times5)})/\omega_{\max(1\times1\times5)}\}$ is always less than 1%, for all initial aspect ratios. In conclusion, provided that a reduction factor of 0.9 is applied to the time step size, the small error magnitude allows to safely use the maximum eigenfrequency $\omega_{\max(1\times1\times1)}$, computed for the uniform strain hexahedron, for the determination of the stable time step size when a different type of element is used in the actual mesh. In the specific case of reduced integration solid-shell elements, the approximation is more favorable and a reduction of 1% only can be adopted. The obtained results are summarized in Table III

In view of this result, the next Section will be devoted to the formulation of an effective strategy for the computation of the maximum eigenfrequency of a solid-shell element integrated with only one Gauss point and with masses selectively scaled according to the procedure illustrated in Section 2.3.

3.2. Equivalent internal nodal forces for one integration point

The use of only one integration point located at the element centroid, greatly simplifies the expression of the equivalent internal nodal forces. Let the subscript 0 denote quantities evaluated at the element centroid $\boldsymbol{\xi}_0 = [0\,0\,0]^T$. The following definitions hold

$$\mathbf{N}_0 = \frac{1}{8}\mathbb{1}_8, \quad \left.\frac{\partial \mathbf{N}^T}{\partial \boldsymbol{\xi}}\right|_{\boldsymbol{\xi}=\boldsymbol{\xi}_0} = \frac{1}{8}\boldsymbol{\xi}_{\square}, \quad \mathbf{J}_0 = \frac{1}{8}\mathbf{X}\boldsymbol{\xi}_{\square}^T, \quad \mathbf{B}_0 = \frac{1}{8}\mathbf{J}_0^{-T}\boldsymbol{\xi}_{\square} \tag{73}$$

where $\boldsymbol{\xi}_{\square}$ is defined in (10). The element volume in (24) is approximated as

$$V_0 = 8J_0 \tag{74}$$

where $J_0 = J(\xi = 0, \eta = 0)$. With these definitions, the equivalent nodal forces turn out to be given by

$$\mathbf{F}_0^{int} = V_0\boldsymbol{\sigma}_0\mathbf{B}_0 = V_0\left[\lambda\left(\mathbf{U}:\mathbf{B}_0\right)\mathbf{I}_3 + \mu\left(\mathbf{U}\mathbf{B}_0^T + \mathbf{B}_0\mathbf{U}^T\right)\right]\mathbf{B}_0$$
$$-\bar{\mathbf{F}}_0^i = \frac{V_0\rho_0}{8}\ddot{\mathbf{U}} \tag{75}$$

where $\boldsymbol{\sigma}_0_{3\times3}$ is the constant stress field evaluated at the element centroid and, as before, a superposed bar means mass lumping. Application of the coordinates transformation (16) and (17) and of the

definition (10) of $\boldsymbol{\xi}_{\square}$ allows to write the Jacobian operator $\mathbf{J}_0$ as

$$\mathbf{J}_0 = \frac{1}{8}\mathbf{X}\boldsymbol{\xi}_{\square}^T = \frac{1}{8}\hat{\mathbf{X}}\mathbf{Q}\boldsymbol{\xi}_{\square}^T = \frac{1}{8}\hat{\mathbf{X}}\hat{\boldsymbol{\xi}}_{\square}^T \tag{76}$$

where $\hat{\boldsymbol{\xi}}_{\square} = \boldsymbol{\xi}_{\square}\mathbf{Q}^T$ is given by

$$\hat{\boldsymbol{\xi}}_{\square} = 2\begin{bmatrix} -1 & 1 & 1 & -1 & 0 & 0 & 0 & 0 \\ -1 & -1 & 1 & 1 & 0 & 0 & 0 & 0 \\ 0 & 0 & 0 & 0 & 1 & 1 & 1 & 1 \end{bmatrix}, \quad \hat{\boldsymbol{\xi}}_{\square}\hat{\boldsymbol{\xi}}_{\square}^T = 2\boldsymbol{\xi}_{\square}\boldsymbol{\xi}_{\square}^T = 16\mathbf{I}_3 \tag{77}$$

The constant strain compatibility matrix $\hat{\mathbf{B}}_0$ is defined as

$$\hat{\mathbf{B}}_0 = \mathbf{B}_0\mathbf{Q}^T = \frac{1}{8}\mathbf{J}_0^{-T}\hat{\boldsymbol{\xi}}_{\square}, \quad \hat{\mathbf{B}}_0\hat{\mathbf{B}}_0^T = \frac{1}{4}\mathbf{J}_0^{-T}\mathbf{J}_0^{-1} = \frac{1}{4}\mathbf{c}_0 \tag{78}$$

If also the nodal dofs are transformed as in (34) and (35), using (18)$_3$ and (38), transformed internal and inertia forces $\mathbf{F}_0^{int}$ and $-\bar{\mathbf{F}}_0^i$ are written as

$$\hat{\mathbf{F}}_0^{int} = V_0\boldsymbol{\sigma}_0\hat{\mathbf{B}}_0 = V_0\left[\lambda\left(\hat{\mathbf{U}}:\hat{\mathbf{B}}_0\right)\mathbf{I}_3 + \mu\left(\hat{\mathbf{U}}\hat{\mathbf{B}}_0^T + \hat{\mathbf{B}}_0\hat{\mathbf{U}}^T\right)\right]\hat{\mathbf{B}}_0$$
$$-\hat{\bar{\mathbf{F}}}_0^i = \frac{V_0\rho_0}{4}\ddot{\hat{\mathbf{U}}} \tag{79}$$

Selective mass scaling is applied as in (45), multiplying by α the lower diagonal block of the lumped mass matrix, leading to

$$-\left(\hat{\bar{\mathbf{F}}}_0^i\right)^\alpha = \frac{V_0\rho_0}{4}\ddot{\hat{\mathbf{U}}}\mathbf{I}_8^\alpha \tag{80}$$

As in (50), the scaling can be partially transferred from the inertia forces to the internal forces, obtaining

$$\delta\hat{\mathbf{U}}^{\sqrt{\alpha}} : \left[-\left(\hat{\bar{\mathbf{F}}}_0^i\right)^{\sqrt{\alpha}} + \left(\hat{\mathbf{F}}_0^{int}\right)^{\frac{1}{\sqrt{\alpha}}}\right] = \mathbf{0} \quad \forall\delta\hat{\mathbf{U}}^{\sqrt{\alpha}} \tag{81}$$

where

$$-\left(\hat{\bar{\mathbf{F}}}_0^i\right)^{\sqrt{\alpha}} = \frac{V_0\rho_0}{4}\ddot{\hat{\mathbf{U}}}\mathbf{I}_8^{\sqrt{\alpha}}$$
$$\left(\hat{\mathbf{F}}_0^{int}\right)^{1/\sqrt{\alpha}} = V_0\left[\lambda\left(\hat{\mathbf{U}}^{\sqrt{\alpha}}:\hat{\mathbf{B}}_0^{1/\sqrt{\alpha}}\right)\mathbf{I}_3 + \mu\left(\hat{\mathbf{U}}^{\sqrt{\alpha}}\left(\hat{\mathbf{B}}_0^{1/\sqrt{\alpha}}\right)^T + \hat{\mathbf{B}}_0^{1/\sqrt{\alpha}}\left(\hat{\mathbf{U}}^{\sqrt{\alpha}}\right)^T\right)\right]\hat{\mathbf{B}}_0^{1/\sqrt{\alpha}} \tag{82}$$

and

$$\hat{\mathbf{B}}_0^{1/\sqrt{\alpha}} = \hat{\mathbf{B}}_0\mathbf{I}_8^{1/\sqrt{\alpha}} = \frac{1}{8}\mathbf{J}_0^{-T}\hat{\boldsymbol{\xi}}_{\square}\mathbf{I}_8^{1/\sqrt{\alpha}} \tag{83}$$

Noting that

$$\mathbf{I}_8^{\sqrt{\alpha}}\hat{\boldsymbol{\xi}}_{\square}^T = \hat{\boldsymbol{\xi}}_{\square}^T\mathbf{I}_3^{\sqrt{\alpha}}, \quad \mathbf{I}_3^{\sqrt{\alpha}} = \begin{bmatrix} 1 & 0 & 0 \\ 0 & 1 & 0 \\ 0 & 0 & \sqrt{\alpha} \end{bmatrix} \tag{84}$$

using (76), one can define

$$\mathbf{J}_0^{\sqrt{\alpha}} = \mathbf{J}_0\mathbf{I}_3^{\sqrt{\alpha}} = \frac{1}{8}\hat{\mathbf{X}}\hat{\boldsymbol{\xi}}_{\square}^T\mathbf{I}_3^{\sqrt{\alpha}} = \frac{1}{8}\hat{\mathbf{X}}\mathbf{I}_8^{\sqrt{\alpha}}\hat{\boldsymbol{\xi}}_{\square}^T = \frac{1}{8}\hat{\mathbf{X}}^{\sqrt{\alpha}}\hat{\boldsymbol{\xi}}_{\square}^T \tag{85}$$

where $\hat{\mathbf{X}}^{\sqrt{\alpha}} = \hat{\mathbf{X}}\mathbf{I}_8^{\sqrt{\alpha}} = [\mathbf{X}^m \ \sqrt{\alpha}\Delta\mathbf{X}]$ is a vector of selectively scaled nodal coordinates, describing an element having the same in-plane geometry, but linearly enlarged in the thickness direction. Using the result in (85) and the definition in (83), matrix $\hat{\mathbf{B}}_0^{1/\sqrt{\alpha}}$ can be expressed as

$$\hat{\mathbf{B}}_0^{1/\sqrt{\alpha}} = \frac{1}{8}\mathbf{J}_0^{-T}\hat{\boldsymbol{\xi}}_{\square}\mathbf{I}_8^{1/\sqrt{\alpha}} = \frac{1}{8}\mathbf{J}_0^{-T}\mathbf{I}_3^{1/\sqrt{\alpha}}\hat{\boldsymbol{\xi}}_{\square} = \frac{1}{8}\left(\mathbf{J}_0^{\sqrt{\alpha}}\right)^{-T}\hat{\boldsymbol{\xi}}_{\square} \tag{86}$$

so that the selectively scaled internal forces $\left(\hat{\mathbf{F}}_0^{int}\right)^{1/\sqrt{\alpha}}$ in (82) can be viewed as obtained from an element with enlarged geometry in the thickness direction. This observation allows to establish an equivalence between the mass scaling and an increase of the element thickness, a concept which will be used in the next sections for the definition of the optimal value of the scaling parameter.

3.3. Formulation of the eigenvalue problem

Considering the eigenvalue problem (81) and assuming a periodic, harmonic evolution in time of the displacement dofs, in view of the linearity of the problem one can write

$$\hat{\mathbf{U}}^{\sqrt{\alpha}}(t) = \hat{\mathbf{V}}^{\sqrt{\alpha}} \sin \omega t, \quad \ddot{\hat{\mathbf{U}}}^{\sqrt{\alpha}}(t) = -\omega^2 \hat{\mathbf{V}}^{\sqrt{\alpha}} \sin \omega t, \quad \boldsymbol{\sigma}_0(t) = \mathbf{s}_0 \sin \omega t \tag{87}$$

With these definitions, the internal and inertia nodal forces become

$$\left(\hat{\mathbf{F}}_0^{int}\right)^{1/\sqrt{\alpha}} = V_0 \mathbf{s}_0 \hat{\mathbf{B}}_0^{1/\sqrt{\alpha}} \sin \omega t$$
$$= V_0 \left[\lambda \left(\hat{\mathbf{V}}^{\sqrt{\alpha}} : \hat{\mathbf{B}}_0^{1/\sqrt{\alpha}} \right) \mathbf{I}_3 + \mu \left(\hat{\mathbf{V}}^{\sqrt{\alpha}} \left(\hat{\mathbf{B}}_0^{1/\sqrt{\alpha}}\right)^T + \hat{\mathbf{B}}_0^{1/\sqrt{\alpha}} \left(\hat{\mathbf{V}}^{\sqrt{\alpha}}\right)^T \right) \right] \hat{\mathbf{B}}_0^{1/\sqrt{\alpha}} \sin \omega t$$
$$\left(\bar{\bar{\hat{\mathbf{F}}}}_0^i\right)^{\sqrt{\alpha}} = \omega^2 \frac{V_0 \rho_0}{4} \hat{\mathbf{V}}^{\sqrt{\alpha}} \sin \omega t$$

$$\tag{88}$$

and the eigenvalue problem (81) admits eigenvectors of the form

$$\hat{\mathbf{V}}^{\sqrt{\alpha}} = \frac{4}{\omega^2 \rho_0} \mathbf{s}_0 \mathbf{B}_0^{1/\sqrt{\alpha}} \tag{89}$$

Since $\mathbf{B}_0^{1/\sqrt{\alpha}}$ has independent rows and is determined by the element geometry, substituting the expression (89) of the eigenvector in the r.h.s. of (88), the eigenvalue problem can be reformulated as the problem of finding ω^2 such that

$$\mathbf{s}_0 = \frac{4}{\omega^2 \rho_0} \left\{ \lambda \left[\mathbf{s}_0 : \left(\hat{\mathbf{B}}_0^{1/\sqrt{\alpha}} \left(\hat{\mathbf{B}}_0^{1/\sqrt{\alpha}}\right)^T \right) \right] \mathbf{I}_3 + \mu \left[\mathbf{s}_0 \hat{\mathbf{B}}_0^{1/\sqrt{\alpha}} \left(\hat{\mathbf{B}}_0^{1/\sqrt{\alpha}}\right)^T + \hat{\mathbf{B}}_0^{1/\sqrt{\alpha}} \left(\hat{\mathbf{B}}_0^{1/\sqrt{\alpha}}\right)^T \mathbf{s}_0 \right] \right\} \tag{90}$$

The solution of problem (90) depends on $\hat{\mathbf{B}}_0^{1/\sqrt{\alpha}} \left(\hat{\mathbf{B}}_0^{1/\sqrt{\alpha}}\right)^T$. According to $(86)_2$ and $(77)_2$, one has

$$\hat{\mathbf{B}}_0^{1/\sqrt{\alpha}} \left(\hat{\mathbf{B}}_0^{1/\sqrt{\alpha}}\right)^T = \frac{1}{64} \mathbf{J}_0^{-T} \mathbf{I}_3^{1/\sqrt{\alpha}} \left(\hat{\boldsymbol{\xi}}_{\square} \hat{\boldsymbol{\xi}}_{\square}^T\right) \mathbf{I}_3^{1/\alpha} \mathbf{J}_0^{-1} = \frac{1}{4} \mathbf{J}_0^{-T} \begin{bmatrix} 1 & 0 & 0 \\ 0 & 1 & 0 \\ 0 & 0 & \frac{1}{\alpha} \end{bmatrix} \mathbf{J}_0^{-1} = \frac{1}{4} \mathbf{J}_0^{-T} \mathbf{I}_3^{1/\alpha} \mathbf{J}_0^{-1} \tag{91}$$

Recalling the definition $(85)_1$ of $\mathbf{J}_0^{\sqrt{\alpha}}$, one can also write

$$\hat{\mathbf{B}}_0^{1/\sqrt{\alpha}} \left(\hat{\mathbf{B}}_0^{1/\sqrt{\alpha}}\right)^T = \frac{1}{4} \left(\mathbf{J}_0^{\sqrt{\alpha}}\right)^{-T} \left(\mathbf{J}_0^{\sqrt{\alpha}}\right)^{-1} = \frac{1}{4} \mathbf{c}_0^{1/\alpha} \tag{92}$$

so that, according to the interpretation given in (15), $\hat{\mathbf{B}}_0^{1/\sqrt{\alpha}} \left(\hat{\mathbf{B}}_0^{1/\sqrt{\alpha}}\right)^T = \frac{1}{4} \mathbf{c}_0^{1/\alpha}$ turns out to be proportional to the inverse of the left Cauchy-Green deformation tensor associated to the mapping which transforms the parent $2 \times 2 \times 2$ cube into the current distorted and scaled element. Its spectral decomposition is given by

$$\hat{\mathbf{B}}_0^{1/\sqrt{\alpha}} \left(\hat{\mathbf{B}}_0^{1/\sqrt{\alpha}}\right)^T = \frac{1}{4} \sum_{i=1}^{3} \left(\gamma_i^{1/\sqrt{\alpha}}\right)^2 \mathbf{t}_i^{1/\sqrt{\alpha}} \left(\mathbf{t}_i^{1/\sqrt{\alpha}}\right)^T \tag{93}$$

Defining the matrices $\mathbf{T}^{1/\sqrt{\alpha}}$ and $\boldsymbol{\gamma}^{1/\sqrt{\alpha}}$ as

$$\mathbf{T}^{1/\sqrt{\alpha}} = [\mathbf{t}_1^{1/\sqrt{\alpha}} \ \mathbf{t}_2^{1/\sqrt{\alpha}} \ \mathbf{t}_3^{1/\sqrt{\alpha}}], \quad \mathbf{T}^{1/\sqrt{\alpha}} \left(\mathbf{T}^{1/\sqrt{\alpha}}\right)^T = \mathbf{I}_3, \quad \boldsymbol{\gamma}^{1/\sqrt{\alpha}} = \text{diag}[\gamma_i^{1/\sqrt{\alpha}}] \tag{94}$$

one has

$$\hat{\mathbf{B}}_0^{1/\sqrt{\alpha}} \left(\hat{\mathbf{B}}_0^{1/\sqrt{\alpha}}\right)^T = \frac{1}{4} \mathbf{T}^{1/\sqrt{\alpha}} \left(\boldsymbol{\gamma}^{1/\sqrt{\alpha}}\right)^2 \left(\mathbf{T}^{1/\sqrt{\alpha}}\right)^T, \quad \left(\mathbf{T}^{1/\sqrt{\alpha}}\right)^T \left[\hat{\mathbf{B}}_0^{1/\sqrt{\alpha}} \left(\hat{\mathbf{B}}_0^{1/\sqrt{\alpha}}\right)^T\right] \mathbf{T}^{1/\sqrt{\alpha}} = \frac{1}{4} \left(\boldsymbol{\gamma}^{1/\sqrt{\alpha}}\right)^2 \tag{95}$$

Defining $\mathbf{S}_0 = \left(\mathbf{T}^{1/\sqrt{\alpha}}\right)^T \mathbf{s}_0 \mathbf{T}^{1/\sqrt{\alpha}}$, equation (90) can be projected onto the principal stretch directions by pre and post multiplying both sides by $\left(\mathbf{T}^{1/\sqrt{\alpha}}\right)^T$ and $\mathbf{T}^{1/\sqrt{\alpha}}$, respectively, thus obtaining:

$$\mathbf{S}_0 = \frac{1}{\omega^2 \rho_0} \left\{ \lambda \left[\mathbf{S}_0 : \left(\gamma^{1/\sqrt{\alpha}}\right)^2 \right] \mathbf{I}_3 + \mu \left[\mathbf{S}_0 \left(\gamma^{1/\sqrt{\alpha}}\right)^2 + \left(\gamma^{1/\sqrt{\alpha}}\right)^2 \mathbf{S}_0 \right] \right\} \tag{96}$$

Problem (96) is equivalent to (90) and represents the generalization to the case of selectively scaled masses of the simplified eigenvalue problem formulated by Flanagan and Belytschko in [26] for a uniform strain trilinear 8-node solid element. The inverse of the maximum eigenvalue $\gamma_3^{1/\sqrt{\alpha}}$ defines the shortening of element fibers in the thickness direction and its corresponding eigenvector $\mathbf{t}_3^{1/\sqrt{\alpha}}$ defines the thickness effective orientation, which is in general not clearly defined for an arbitrarily distorted element. Following [26, 20], the maximum eigenvalue ω_{max}^2 of problem (96) corresponds to an extensional vibration mode in the thickness direction, and can be obtained by solving (96) with $\mathbf{S}_0$ describing a purely normal stress state

$$\mathbf{S}_0 = \begin{bmatrix} S_1 & 0 & 0 \\ 0 & S_2 & 0 \\ 0 & 0 & S_3 \end{bmatrix} \tag{97}$$

Defining for notation simplicity $\chi_i = \left(\gamma_i^{1/\sqrt{\alpha}}\right)^2$, with $\chi_1 \le \chi_2 \le \chi_3$, problem (96) can be rewritten as

$$\begin{bmatrix} S_1 \\ S_2 \\ S_3 \end{bmatrix} = \frac{1}{\omega^2 \rho_0} \begin{bmatrix} (\lambda + 2\mu)\chi_1 & \lambda\chi_2 & \lambda\chi_3 \\ \lambda\chi_1 & (\lambda + 2\mu)\chi_2 & \lambda\chi_3 \\ \lambda\chi_1 & \lambda\chi_2 & (\lambda + 2\mu)\chi_3 \end{bmatrix} \begin{bmatrix} S_1 \\ S_2 \\ S_3 \end{bmatrix} \tag{98}$$

or, in terms of the more used Poisson's coefficient ν instead of Lamé's constant λ:

$$\left(\begin{bmatrix} \dfrac{1-\nu}{1-2\nu}\chi_1 & \dfrac{\nu}{1-2\nu}\chi_2 & \dfrac{\nu}{1-2\nu}\chi_3 \\ \dfrac{\nu}{1-2\nu}\chi_1 & \dfrac{1-\nu}{1-2\nu}\chi_2 & \dfrac{\nu}{1-2\nu}\chi_3 \\ \dfrac{\nu}{1-2\nu}\chi_1 & \dfrac{\nu}{1-2\nu}\chi_2 & \dfrac{1-\nu}{1-2\nu}\chi_3 \end{bmatrix} - \dfrac{\omega^2 \rho_0}{2\mu} \begin{bmatrix} 1 & 0 & 0 \\ 0 & 1 & 0 \\ 0 & 0 & 1 \end{bmatrix} \right) \begin{bmatrix} S_1 \\ S_2 \\ S_3 \end{bmatrix} = \mathbf{0} \tag{99}$$

The characteristic equation of problem (99) is given by the following cubic equation

$$f\left(\omega^2; \alpha\right) = \left(\omega^2\right)^3 - \frac{1-\nu}{1-2\nu}\frac{2\mu}{\rho_0} I_1^{1/\alpha} \left(\omega^2\right)^2 + \frac{1}{1-2\nu}\left(\frac{2\mu}{\rho_0}\right)^2 I_2^{1/\alpha}\, \omega^2 - \frac{1+\nu}{1-2\nu}\left(\frac{2\mu}{\rho_0}\right)^3 I_3^{1/\alpha} = 0 \tag{100}$$

where f is a function of ω^2 parameterized by the value of α and

$$\begin{aligned} I_1^{1/\alpha} &= \chi_1 + \chi_2 + \chi_3 \\ I_2^{1/\alpha} &= \chi_1\chi_2 + \chi_2\chi_3 + \chi_1\chi_3 \\ I_3^{1/\alpha} &= \chi_1\chi_2\chi_3 \end{aligned} \tag{101}$$

are the invariants of $\mathbf{c}_0^{1/\alpha} = \left(\mathbf{J}_0^{\sqrt{\alpha}}\right)^{-T} \left(\mathbf{J}_0^{\sqrt{\alpha}}\right)^{-1} = 4\mathbf{B}_0^{1/\sqrt{\alpha}} \left(\hat{\mathbf{B}}_0^{1/\sqrt{\alpha}}\right)^T$. Since the characteristic equation (100) depends directly on the invariants, the spectral decomposition of $\mathbf{B}_0^{1/\sqrt{\alpha}} \left(\hat{\mathbf{B}}_0^{1/\sqrt{\alpha}}\right)^T$ is not required in practice. These invariants depend only on the element geometry and on the mass scaling parameter, which is embedded in $\mathbf{B}_0^{1/\sqrt{\alpha}}$, as it is clearly shown by equation (83), and can be easily computed for each element in the mesh.

Equation (100) shows that, in the present one-Gauss-point approach, the element maximum eigenfrequency depends only on the mass scaling and on the principal values γ_i. This means that different elements, with different distortions, but characterized by the same γ_i, lead to the same stable time step. It is therefore difficult to establish a connection between element distortion and maximum eigenfrequency.
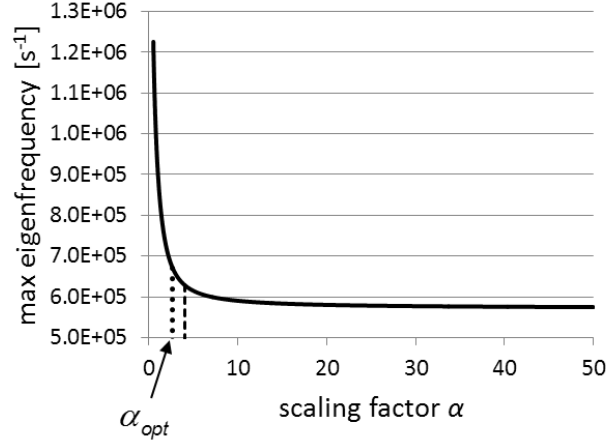
Figure 4. Decrease of max eigenfrequency ω_{max} for increasing scaling factor α and optimal values of scaling factor: rigorous estimate $\alpha_{opt} = 2.68$, dots; simplified estimate $\alpha_{opt} = 4.07$, dashes.

3.4. Optimal value of mass scaling parameter

On the basis of equations (100) and (2), the problem of the definition of the critical time step is reduced to the computation of the largest root of the third order equation (100). This however requires the definition of the scaling parameter α. Furthermore, one has to take into account that in large deformation problems, where the linear stability criterion (2) is usually applied in conjunction with a safety reduction factor and an energy stability check, when the element geometry changes significantly during the deformation process, ω_{max} has to be computed repeatedly for each element, so that the analytical solution of (100) turns out to be too expensive.

The decrease of ω_{max} for increasing α is shown in Figure 4 for the element of the $p2$ family of Section 2.3, shown in Figure 2. It can be seen that for small values of α there is a significant gain, which decreases rapidly for moderate values of α. For large values of α, ω_{max} tends asymptotically to a constant value ω_∞, which can be easily computed by letting $\alpha \to \infty$ in $f\left(\omega^2; \alpha\right)$ in (100). ω_∞ represents a lower bound on ω_{max}, which can be approached only at the cost of very large mass scaling, with consequent loss of accuracy in the description of the structural motion. In [13], it was empirically proposed to take $\omega_{target} = \omega_\infty / 0.9$ as a target value and to compute α from $f\left(\omega_{target}^2; \alpha\right) = 0$.

A more rationale criterion for the definition of α can be obtained by considering the equivalence between mass and geometric scalings proved in (86). It has been shown that the maximum eigenfrequency is associated to the thickness vibration mode and that it increases linearly with the inverse of the thickness. On the other hand, for a perfectly cubic element, the three roots of (100) are identical. This consideration naturally leads to the formulation of a simple criterion for the selection of the optimal value of the scaling parameter: the optimal scaling α_{opt} should be the one making the thickness to become of a size comparable with the in-plane dimensions. For a highly distorted element, a rigorous procedure would consists of carrying out the spectral decomposition (15) of $\mathbf{c}_0$, where $\mathbf{c}_0$ is defined in (78), choosing the direction of $\mathbf{t}_3$ as the thickness direction and setting $\alpha_{opt} = \left(\gamma_3 / \gamma_2\right)^2$ for each element e. This computation has to be carried out only once, before starting the analysis, and therefore is not computationally invasive.

As an alternative, the following simplified inexpensive approach can be followed. For each element, define approximate in-plane dimensions and thickness L_1, L_2, h_0, respectively, as the distances between the centroids of element faces, i.e.:

$$L_1 = \|\mathbf{x}(1,0,0) - \mathbf{x}(-1,0,0)\|, \ L_2 = \|\mathbf{x}(0,1,0) - \mathbf{x}(0,-1,0)\|, \ h_0 = \|\mathbf{x}(0,0,1) - \mathbf{x}(0,0,-1)\|$$
(102)

Then set

$$\alpha_{opt} = \frac{L_{min}^2}{h_0^2}, \quad L_{min} = \min\{L_1, L_2\} \tag{103}$$

The two estimates would provide the same result for a parallelepiped element. As shown in Figure 4, using (103) for the significantly distorted and relatively thick element of the $p2$ family in Figure 2, one obtains a moderate mass scaling factor $\alpha_{opt} = 4.07$, while the rigorous procedure based on the spectral decomposition (15) provides $\alpha_{opt} = 2.68$. Much higher values are obtained for thinner elements, as it will be shown in the numerical examples.

For this particular type of distortion, the two estimates are significantly different, but looking at the plot in Figure 4, one can see that in both cases α_{opt} defines a maximum eigenfrequency well within the curved part of the plot. A numerical study, considering the three families of distorted elements defined in Section 2.3, shows that the average difference between the two estimates is about 10-13%, depending on the reference thickness.

Considering the estimate in (103), it is interesting to note that, in view of the adopted one-Gauss-point integration, all elements having the same L_1, L_2, h_0 measuring orthogonal segments, no matter what is their distortion, have the same γ_1, γ_2, γ_3 and, hence, the same ω_{max}. In other words, if a parallelepiped element of edges L_1, L_2, h_0 is distorted in such a way that the segments connecting the centroids of its opposite facets do not change in length and remain orthogonal, then its ω_{max} remains the same.

After the optimal value of α has been defined, one has to compute ω_{max}^α in an accurate and inexpensive way for each element in the mesh, whenever the element distortion is such to require a new computation. As an initial tentative value of ω_{max}^α for a given element, an upper bound ω_G^α on the element maximum eigenfrequency can be computed using Gershgorin's estimate applied to the eigenvalue problem (99). According to Gershgorin's theorem [25], an upper bound on a matrix maximum eigenvalue is given by the maximum value obtained by summing up the modules of the entries of each row of the matrix. In the case of the matrix in (99), this gives

$$\omega_{max}^2 \leq \omega_G^2 = \frac{2\mu}{\rho_0}\left[\frac{\nu}{1-2\nu}I_1^{1/\alpha} + \max_i\left\{\sum_{j=1}^3\left|[\mathbf{c}_0^{1/\alpha}]_{ij}\right|\right\}\right] \tag{104}$$

Since the matrix is not symmetric, a different estimate could be obtained also by summing up the modules of the entries of each column. However, it can be shown that for the matrix in (99) the sharper bound is always given by the row sum, which is therefore used hereafter. The bound in (104) can be overly large for practical use. A sharper bound can be easily obtained performing a Newton-Raphson iteration on the characteristic equation $f\left(\omega^2;\alpha^{opt}\right)$, starting from the initial value ω_G^2

$$\omega_{N-R}^2 = \omega_G^2 - \frac{f\left(\omega_G^2;\alpha^{opt}\right)}{f'\left(\omega_G^2;\alpha^{opt}\right)} \tag{105}$$

where

$$f'\left(\omega_G^2;\alpha\right) = 3(\omega_G^2)^2 - 2\frac{1-\nu}{1-2\nu}\frac{2\mu}{\rho_0}I_1^{1/\alpha}(\omega_G^2) + \frac{1}{1-2\nu}\left(\frac{2\mu}{\rho_0}\right)^2 I_2^{1/\alpha} \tag{106}$$

The estimate in (106) is still an upper bound, and hence conservative as far as time integration stability is concerned, and is rather sharp and less expensive than the analytical solution of the cubic equation in (100). An example of the iterative procedure applied to the element in Figure 2 with $\alpha = 2.68$ is shown in Figure 5, where the following values have been obtained: $\omega_G^2 = 0.749$ s^{-2}, $\omega_{N-R}^2 = 0.677$ s^{-2}, $\omega_{exact}^2 = 0.655$ s^{-2}, with a final error from above of 1.7% on ω_{max}. The numerical investigation on the 3×10000 elements of Section 2.3 gives a maximum error (always from above) of about 3% for all the three element families $p2$, $p5$, $p10$, while the average error is of about 1%. The procedure to be followed for the computation of ω_{max} is summarized in Box 1.

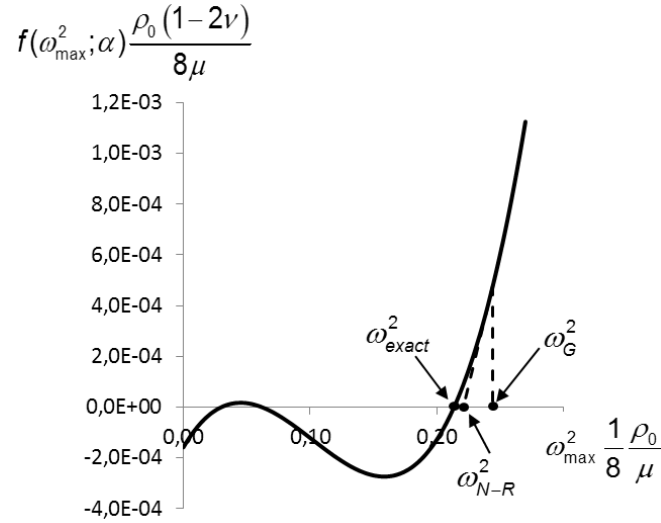$$f(\omega_{max}^2;\alpha)\frac{\rho_0(1-2\nu)}{8\mu}$$

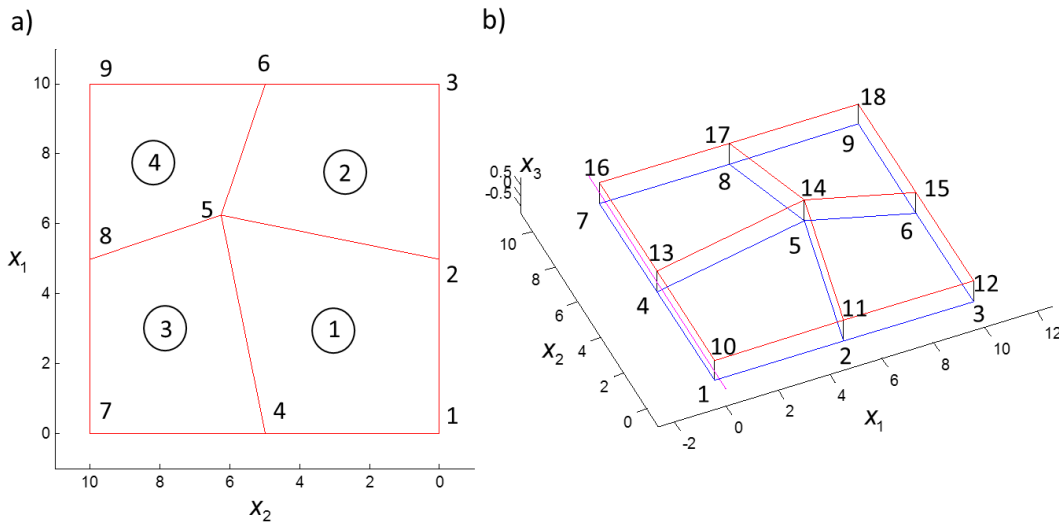Figure 5. One-iteration procedure for estimate of ω_{max}^2.

Figure 6. Rotational patch-test: distorted element patch. a) patch lower surface; b) three-dimensional view.

4. NUMERICAL EXAMPLES

4.1. Rotational patch test

In Section 2.5 it has been shown how the proposed selective mass scaling alters the rotational inertia of a parallelepiped element. A similar result is expected also with distorted elements. To test numerically the impact of the mass scaling in this case, the square patch of four distorted elements shown in Figure 6 is considered. Other types of patch tests, specifically conceived for testing mass matrices, have been proposed in [30], chapt. 5.

The test setup is as in Section 2.5, i.e. the patch is forced to rigidly rotate around the x_2 axis with constant angular velocity $\dot{\beta}$ and the patch centroid G is assumed to be placed at a distance r_G from the rotation axis. The patch is a square parallelepiped with side $L = 10$ mm and thickness $h = 1$ mm (i.e. $\gamma = L/h = 10$). The distorted mesh has been obtained starting from a regular mesh of four square elements and displacing the central nodes (5 and 14 in Figure 6) along the patch diagonal,

node	X_1	X_2	X_3
5	6.25	6.25	-0.5
14	6.25	6.25	0.5

Table IV. Rotational patch test: coordinates of central nodes.

e	α^e_{opt}	Δt^e	$\bar{\alpha}^e_{opt}$	$\Delta \bar{t}^e$
1	25.00	7.95×10^{-2}	10.21	6.03×10^{-2}
2	19.48	7.06×10^{-2}	11.06	6.03×10^{-2}
3	19.48	7.06×10^{-2}	11.06	6.03×10^{-2}
4	14.06	6.03×10^{-2}	14.06	6.03×10^{-2}

Table V. Rotational patch test: optimal values of α and critical time step.

so that they now have the coordinates shown in Table IV. To contrast the centrifugal inertia force, a centripetal body force of the same magnitude and opposite direction is applied to the elements in the patch. Upon discretization, equivalent nodal forces are applied to the two unconstrained central nodes of the patch (nodes 5 and 14 in Figure 6). For uniform angular velocity ($\ddot{\beta} = 0$), the acceleration field is given by

$$\mathbf{\ddot{u}} = \mathbf{\ddot{R}}\mathbf{x}_0 = -\dot{\beta}^2 \begin{bmatrix} \cos\beta & 0 & -\sin\beta \\ 0 & 0 & 0 \\ \sin\beta & 0 & \cos\beta \end{bmatrix} \mathbf{x}_0 \tag{107}$$

where $\mathbf{x}_0$ defines the original configuration and $\mathbf{R}$ is defined in (53).

The centripetal forces are obtained on each element as

$$\mathbf{F}^c = \mathbf{\ddot{U}} \int_{\Omega^e} \rho \mathbf{N}\mathbf{N}^T \, d\Omega, \quad \mathbf{\ddot{U}} = \mathbf{\ddot{R}}\mathbf{X}_0 \tag{108}$$

If a consistent mass matrix is used, the inertia forces are exactly compensated, and a perfectly rigid motion, with constant kinetic energy, is obtained (to within the approximation error induced by the central difference time integration). This is not the case if the lumped mass matrix in (40) is used. As a consequence, a slightly oscillating kinetic energy, together with a non-zero elastic energy is obtained. An additional error is introduced when the selectively scaled mass matrix in (45) is used.

As a first step, the optimal value α^e_{opt} of the scaling factor is computed for each element, solving the eigenvalue problem in (15). The optimal values obtained for the four elements are shown in the second column of Table V, together with the corresponding stable time steps Δt^e. The Δt_{crit} to be used for the time integration of the assembled patch is the smallest among them, i.e. $\Delta t_{crit} = \min_e \Delta t^e = \Delta t^4$. For the three elements with $\Delta t^e \geq \Delta t_{crit}$, the adopted mass scaling is larger than needed, with a useless accuracy loss. To overcome the problem, for these elements α^e_{opt} is recomputed from (100) where, this time, ω has been replaced by $2/\Delta t_{crit}$, obtaining the values $\bar{\alpha}^e_{opt}$ shown in the fourth column in Table V. In this way, the same $\Delta \bar{t}^e = \Delta t_{crit}$ is obtained for all elements (see $\Delta \bar{t}$ in the fifth column of Table V), with optimal mass scaling application. Even though this second loop over the elements can appear computationally expensive, it should be noted that this computation has to be carried out only once at the beginning of the analysis.

Three different cases are considered, with patch rotations assigned around three axes, parallel to x_2, at increasing distance r_G from the patch centroid, with $r_G/L = 0.5$, 2, 3.5. For the same angular velocity, as r_G/L increases, the motion translational component also increases, while the rotational one remains constant. Snapshots of the three motions are shown in Figure 7, for the same centroid position. The elastic energy $\bar{\bar{\mathcal{E}}}^\alpha - \bar{\mathcal{E}}$ generated by the mass scaling in addition to the one due to the use of a lumped mass matrix is negligibly small if compared to the kinetic energy (note that all these energies depend on $\dot{\beta}^2$ and therefore their ratio is independent of the
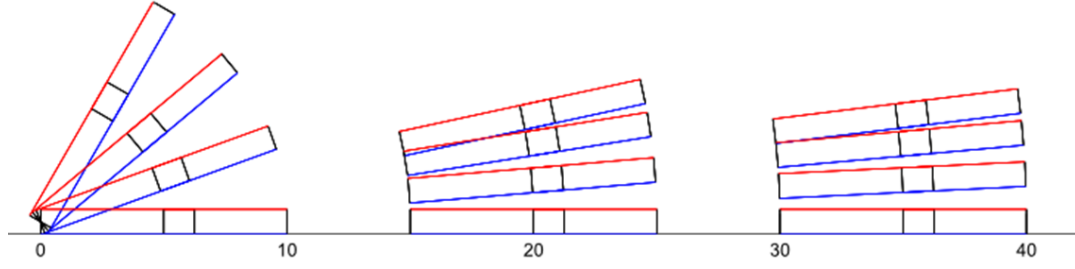
Figure 7. Rotational patch-test: patch rotation around three different axes. Snapshots at same centroid elevations.

$\dfrac{r_G}{L}$	$\dfrac{\hat{\bar{\mathcal{E}}}^\alpha - \bar{\mathcal{E}}}{\bar{K}}$	$\dfrac{\hat{\bar{K}}^\alpha - \bar{K}}{\bar{K}}$	$\bar{e}$
0.5	1.40×10^{-4}	6.79×10^{-2}	6.47×10^{-2}
2	1.30×10^{-5}	7.42×10^{-3}	7.64×10^{-3}
3.5	4.33×10^{-6}	3.33×10^{-3}	2.60×10^{-3}

Table VI. Rotational patch test. Elastic and kinetic energy errors (column 2 and 3) and estimated value $\bar{e}$ (72) of kinetic energy error (column 4).

assigned rotation velocity), as shown in the second column of Table VI. Since the translational motion component is purely rigid, the elastic energy depends only on the rotational part of the motion and $\hat{\bar{\mathcal{E}}}^\alpha - \bar{\mathcal{E}}$ is constant for increasing ratio r_G/L, while $\bar{K}$ increases, implying that the small error in column 2 tends to decrease asymptotically with the square of r_G/L, as much as the error on the kinetic energy, reported in column 3. Since the energies computed with the lumped mass matrix are slightly oscillating, differences between maximum values are shown in columns 2 and 3 of Table VI. The error $\bar{e}$ estimated using (72) is reported in column 4. Since α and γ in (72) are in principle different for each element, α and γ pertaining to element 4, the one dictating the critical time step, are used. Since in this case $\alpha_{opt} = (\gamma_3/\gamma_2)^2$ is used, one has $\alpha = \gamma^2$ in (72) and, hence $\bar{e} = (1 - \alpha)/\alpha \cdot (L/4r_G)^2$, where $L = 10$ mm is the length of the patch side. This is the value reported in Table VI. It can be noted that in all cases $\bar{e}$ provides a reasonable estimate of the order of magnitude of the error on the kinetic energy.

4.2. Impulsively loaded cantilever: small displacements

The cantilever beam depicted in Figure 8 has been used in [13] to discuss the effectiveness of the selective mass scaling for parallelepiped elements and it is used here with distorted elements. The beam has a side length of $l = 6000$ mm and a width of $w = 200$ mm. Four thicknesses are considered: $h = 10$, $h = 25$, $h = 50$, $h = 100$ mm. In the thinnest case, the element width to thickness ratio is 20. The cantilever is made of steel. The material parameters are: $E = 200000$ N/mm^2 (Young's modulus), $\nu = 0.3$ (Poisson's ratio) and $\rho = 7.5 \cdot 10^{-9}$ Ns^2/mm^4 (mass density). A constant concentrated tip load F is applied in the vertical direction, equally distributed among the four tip nodes. To remain in the small displacement range for all thicknesses and to obtain comparable curves, the applied load has been scaled in each case so as to obtain the same static tip displacement: $F = 500$, $F = 62.5$, $F = 7.8125$, $F = 0.5$ N. Results are discussed in terms of the tip displacement. As a reference, the analytical static solution is $v_{\mathrm{ref}} = 10.8$ mm for all thicknesses. The structure is discretized by means of 6 distorted Q1STs solid-shell elements [8] over the length l. In the other two directions only one element is used (Figure 8b).

For each thickness, the simplified formula in (103) has been used to compute the optimal value of the mass scaling parameter for each element, while the procedure in Box 1 has been used for the determination of the maximum element eigenfrequency and, hence, of the critical time step
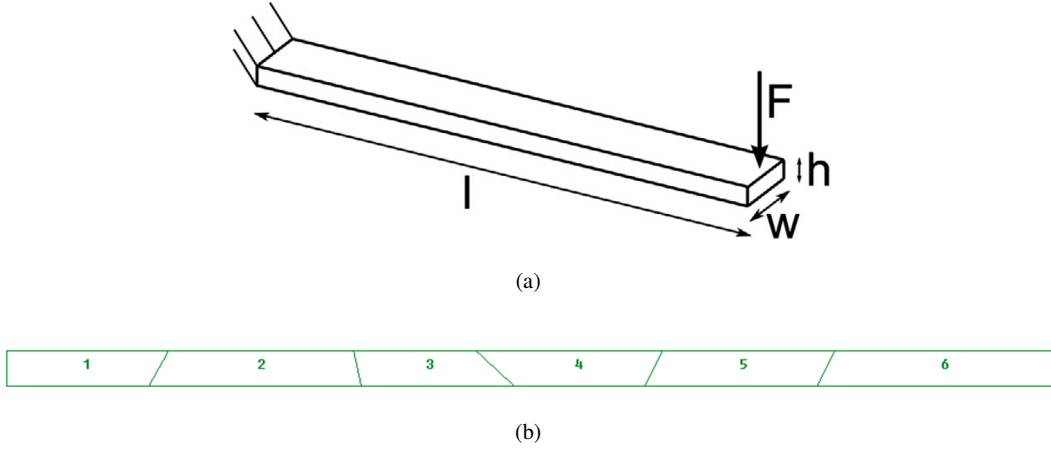
(a)

(b)

Figure 8. Linear cantilever beam. a) Geometry and boundary conditions. b) Finite element mesh.

e	$h = 10$ mm	$h = 25$ mm	$h = 50$ mm	$h = 100$ mm
1	430.80	68.93	17.23	4.31
2	411.56	65.85	16.46	4.12
3	570.30	91.25	22.81	5.70
4	434.81	69.57	17.39	4.35
5	499.00	79.84	19.96	4.99
6	424.50	67.92	16.98	4.25

Table VII. Linear cantilever beam. Optimal values of mass scaling factor α.

	$h = 10$ mm	$h = 25$ mm	$h = 50$ mm	$h = 100$ mm
$\Delta t^{(\alpha=1)}$	1.67E-06	4.00E-06	8.29E-06	1.62E-05
$\Delta t^{(\alpha=\alpha_{opt})}$	2.80E-05	2.75E-05	2.80E-05	2.80E-05
e_{crit}	2	2	2	2

Table VIII. Linear cantilever beam. Critical time step with and without mass scaling. e_{crit} denotes the element determining the critical time step.

according to (2). The obtained values of the scaling parameter are listed in Table VII for each element and thickness. As expected, the optimal scaling decreases as the thickness increases and slightly varies among elements of the same thickness, depending on the different in-plane distortion.

The stable time step for the different thicknesses and with and without mass scaling is shown in Table VIII. The critical time step is the minimum among the critical time steps associated to individual elements. In this case, element 2 turns out to be the critical one for all thicknesses. One can also observe that the obtained stable time step is practically the same for all thicknesses and therefore it is determined by the element in-plane geometry only. The gain with respect to the case of unscaled masses (compare the rows "$\Delta t^{(\alpha=1)}$" and "$\Delta t^{(\alpha=\alpha_{opt})}$"), increases as the thickness decreases, becoming larger than one order of magnitude in the thinnest case. Despite the large mass scaling, which in the thinnest case is more than 400, the accuracy loss is negligible. Figure 9a shows the curves obtained for the different thicknesses in terms of tip displacement. Due to the reduced stiffness, the beam first eigenperiod increases linearly with the thickness reduction. To obtain a thickness independent response, the same curves are plotted in Figure 9b, against a time scaled by the beam first eigenperiod T. The curves are superposed and no effects of the scaling can be observed. In conclusions, the proposed selective mass scaling produces only negligible modifications of the structure dynamical response in the case of small displacements and rotations.
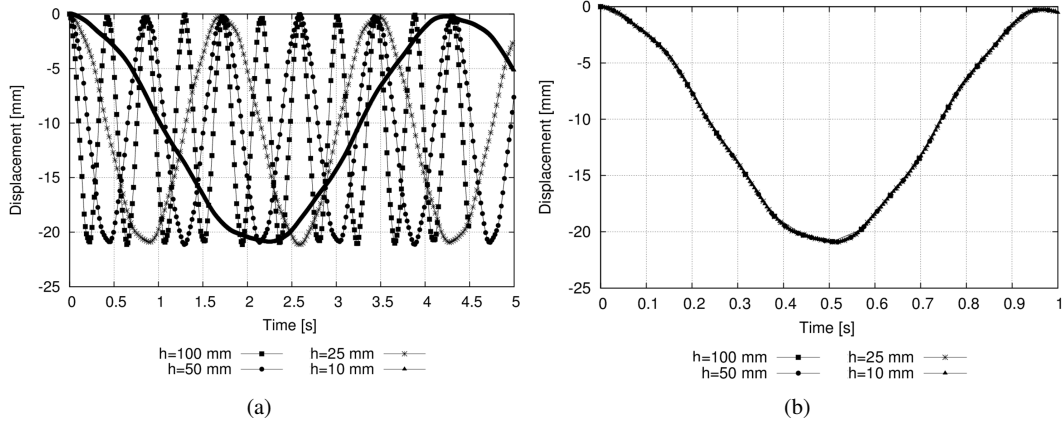
Figure 9. Linear cantilever beam. (a) Tip displacement for varying thickness and mass scaling. (b) Same as (a) with scaled time. Mass scaling parameters values are reported in Table VII.

	$h = 10$ mm	$h = 25$ mm	$h = 50$ mm	$h = 100$ mm	e
α_{opt}^{max}	146.67	23.47	5.87	1.47	13
α_{opt}^{min}	39.00	6.24	1.56	1.00	15

Table IX. Large displacement cantilever beam. Maximum and minimum values of α_{opt}.

4.3. Impulsively loaded cantilever: large displacements

To test the loss of accuracy implied by the selective mass scaling in the case of large displacements, a cantilever beam subjected to a much higher load $F = 3600$ N is considered. The test setup is the same as in Figure 8, but in this case dimensions $l = 2000$ mm, $w = 200$ mm and $h = 10, 25, 50, 100$ mm have been considered, and the distorted mesh in Figure 10, with two Q1STs solid-shell elements along the width and ten along the length, has been used. The different geometry has been chosen in order to test the effect of mass scaling in the presence of more severe element distortion.
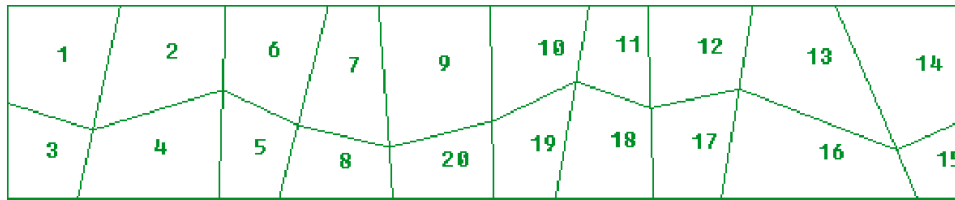

Figure 10. Large displacement cantilever beam. Finite element mesh.

In the thickest beam ($h = 100$ mm), for many elements (9-14, 16-18, 21-26) the smallest in-plane dimension is smaller than the thickness and the resulting α_{opt} is equal to one. The highest value resulting from the application of the simplified procedure in (103) is for element 13, with $\alpha_{opt} = 1.47$. Maximum and minimum values of α_{opt} for the different thicknesses, are reported in Table IX, together with the corresponding element number.

The stable time step for the different thicknesses, with and without mass scaling is shown in Table X. In the case $h = 100$ mm, the critical time step remains unchanged. This is due to the fact that the critical time step is dictated by element 15 and, for this element, an in-plane dimension is the smallest one. Therefore, $\alpha_{opt} = 1$ is used, so that no mass scaling is applied. Since a finer mesh is used in this case, the gain in terms of time step size is much smaller than in the previous example.

	$h = 10$ mm	$h = 25$ mm	$h = 50$ mm	$h = 100$ mm
$\Delta t^{(\alpha=1)}$	1.66E-06	3.88E-06	6.97E-06	8.48E-06
$\Delta t^{(\alpha=\alpha_{opt})}$	7.75E-06	7.75E-06	7.75E-06	8.48E-06
e_{crit}	15	15	15	15

Table X. Large displacements cantilever beam. Critical time step with and without mass scaling. e_{crit} denotes the element determining the critical time step.

The history of the tip displacement of the thinnest beam ($h = 10$ mm, $\alpha_{opt} = 39.00$) is shown in Figure 11. The maximum tip displacement is more than 50% of the beam length, so that it can certainly be classified as large. Three curves are shown: the curves with and without selective mass scaling and the curve obtained with the finite element code Abaqus, using the same mesh, but made of shell elements of the S4R type. The three curves are almost perfectly superposed, implying that also in this case the translational part of the rigid body motion is largely dominant over the rotational one.
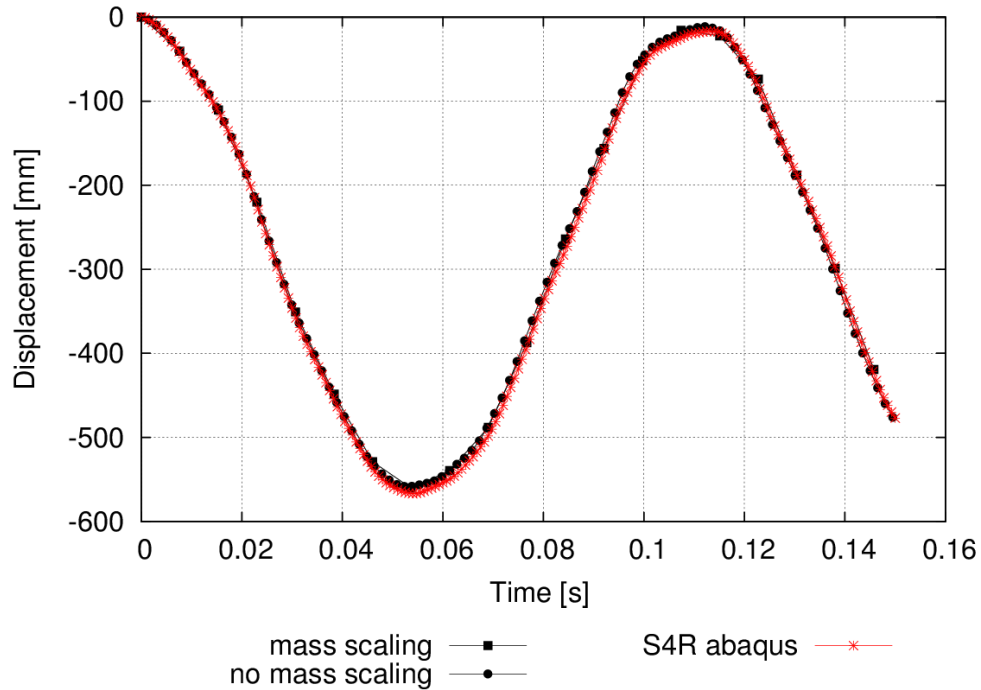

Figure 11. Large displacement cantilever beam. History of tip displacement: with and without selective mass scaling, using Abaqus S4R element mesh.

5. CONCLUSIONS

In explicit dynamics applications with solid-shell elements, the smallness of the thickness with respect to the element in-plane dimensions leads to unacceptably small time step sizes, compromising their effective applicability in this context. In inertia dominated problems, the structural response is predominantly governed by element translational rigid body motions. This aspect has been exploited by several researchers to propose different strategies intended to reduce the element highest eigenfrequencies through selective mass scaling. With solid-shell elements, the goal of the mass scaling is that the critical time step be governed by the element in-plane dimensions and not by the thickness. Furthermore, a highly desirable feature in explicit dynamics is that the adopted

selective mass scaling preserves the mass matrix diagonal structure, a requirement not satisfied by most of the solutions proposed in the literature.

In [20], a selective mass scaling for solid-shell elements of parallelepiped shape was proposed. The mass scaling preserved the element rigid body translational inertia and the mass matrix original diagonal structure leading, upon selection of suitable values of the scaling parameter, to a critical time step size governed by the element in-plane dimensions and not anymore by the element thickness. In the present work, the selective mass scaling method proposed in [20] has been applied to solid-shell elements of arbitrary distorted shape. Two critical aspects have been addressed in particular: the definition of a criterion for the optimal choice of the scaling factor; the definition of a computationally effective approach for the computation of the distorted element maximum eigenfrequency and, hence, of the assembled mesh critical time step size.

Following the approach proposed in [26], reference has been made to a one-Gauss point, 8-node solid element. The applicability of the results obtained for the underintegrated element to other types of solid-shell elements has been assessed through a numerical verification campaign. For the one-Gauss point element, it has been shown that the proposed selective mass scaling is equivalent to a geometric thickness scaling, providing in this way a clear criterion for the choice of the mass scaling factor optimal value: the mass scaling must be large enough to make the thickness of a size comparable to the smallest in-plane dimension, but not larger. The optimal value of the mass scaling parameter is therefore an element property and its definition can be carried out element by element at the beginning of the analysis, in a pre-processing step. In large strain problems, the element shape can vary significantly during the analysis. While the mass scaling parameter cannot be modified (it would imply an artificial energy modification), the elements maximum eigenfrequencies have to be recomputed run-time. An accurate and computationally effective procedure for the computation of the element maximum eigenfrequency has been proposed to this purpose.

While the translational inertia is not affected, the proposed selective mass scaling modifies the element rotational inertia. The error on the kinetic energy implied by this modification in a rigid body rotational motion has been assessed analytically for a simple case and a closed form formula has been derived for its estimation. A special type of patch test has been designed to asses the energy error due to the scaled rotational inertia for distorted elements. It has been shown that the error tends asymptotically to decrease quadratically as the translational content of the motion grows with respect to the rotational one. On the basis of these results, the proposed selective mass scaling should not be applied in the case of motions dominated by the rotational rigid body component.

Numerical tests with meshes of distorted elements, both in small and large displacements, have shown the accuracy and the effectiveness of the method. In particular, for discretizations exhibiting the same in-plane mesh, it has been shown that for suitable values of the mass scaling factor the same critical time step can be obtained regardless of the thickness, with no appreciable effect on the analysis results. Once the scaling has been applied and the thickness is no longer the critical parameter, other types of mass scaling (see e.g. [15, 18, 19]) can in principle be applied, on the basis of the elements in-plane dimensions, to further increase the allowable time step size.

ACKNOWLEDGMENTS

REFERENCES

1. Belytschko T, Liu WK, Moran B. *Nonlinear finite elements for continua and structures*. Wiley, 2000.
2. Key SW, Beisinger ZE. The transient dynamic analysis of thin shells by the finite element method. *Proc. of the Third Conference on Matrix Methods in Structural Mechanics*, 1971.
3. Hughes TJR, Cohen M, Haroun M. Reduced and selective integration techniques in the finite element analysis of plates. *Nuclear Engineering and Design* Mar 1978; **46**(1):203–222, doi:10.1016/0029-5493(78)90184-X.
4. Hughes TJR. *The Finite Element Method - Linear Static and Dynamic Finite element Analyses*. Prentice-Hall, 1987.
5. Parisch H. A continuum-based shell theory for non-linear applications. *International Journal for Numerical Methods in Engineering* 1995; **38**(11):1855–1883.

6. Hauptmann R, Schweizerhof K. A systematic development of 'solid-shell' element formulations for linear and non-linear analyses employing only displacement degrees of freedom. *International Journal for Numerical Methods in Engineering* 1998; **42**(1):49–69.

7. Vuquoc L, Tan XG. Optimal solid shells for non-linear analyses of multilayer composites. II. dynamics. *Computer Methods in Applied Mechanics and Engineering* Feb 2003; **192**(9-10):1017–1059.

8. Schwarze M, Reese S. A reduced integration solid-shell finite element based on the EAS and the ANS concept: Large deformation problems. *International Journal for Numerical Methods in Engineering* 2011; **85**(3):289–329.

9. Li LM, Li DY, Peng Y. An explicit formulation of solid-shell element and its application in sheet metal forming processes. *Advanced Science Letters* 2011; **4**:1761–1766.

10. Xu HJ, Liu YQ, Zhong W. Three-dimensional finite element simulation of medium thick plate metal forming and springback. *Finite Elements in Analysis and Design* April 2012; **51**:49–58.

11. Mattern S, Schmied C, Schweizerhof K. Incompatible modes for volumetric shell elements in explicit time integration. *PAMM* 2012; **12**(1):181–182, doi:10.1002/pamm.201210081.

12. Pagani M, Reese S, Perego U. Explicit Simulation of Forming Processes Using a Novel Solid-Shell Concept Based on Reduced Integration. *Key Engineering Materials* Feb 2012; **504-506**:425–430, doi:10.4028/www.scientific.net/KEM.504-506.425.

13. Pagani M, Reese S, Perego U. Computationally efficient explicit nonlinear analyses using reduced integration-based solid-shell finite elements. *Computer Methods in Applied Mechanics and Engineering* 2014; **268**:141–159, doi:10.1016/j.cma.2013.09.005.

14. Macek RW, Aubert BH. A mass penalty technique to control the critical time increment in explicit dynamic finite element analyses. *Earthquake Engineering and Structural Dynamics* 1995; **24**(10):1315–1331.

15. Olovsson L, Simonsson K, Unosson M. Selective mass scaling for explicit finite element analyses. *International Journal for Numerical Methods in Engineering* 2005; **63**(10):1436–1445.

16. Askes H, Nguyen D, Tyas A. Increasing the critical time step: micro-inertia, inertia penalties and mass scaling. *Computational Mechanics* Jun 2011; **47**(6):657–667.

17. Hetherington J, Rodrguez-Ferran A, Askes H. A new bipenalty formulation for ensuring time step stability in time domain computational dynamics. *International Journal for Numerical Methods in Engineering* 2012; **90**(3):269–286, doi:10.1002/nme.3314.

18. Tkachuk A, Bischoff M. Variational methods for selective mass scaling. *Computational Mechanics* 2013; **52**(3):563–570, doi:10.1007/s00466-013-0832-0.

19. Tkachuk A, Bischoff M. Local and global strategies for optimal selective mass scaling. *Computational Mechanics* 2014; **53**(6):1197–1207, doi:10.1007/s00466-013-0961-5. URL http://dx.doi.org/10.1007/s00466-013-0961-5.

20. Cocchetti G, Pagani M, Perego U. Selective mass scaling and critical time-step estimate for explicit dynamics analyses with solid-shell elements. *Computers & Structures* 2013; **127**:39–52.

21. Olovsson L, Unosson M, Simonsson K. Selective mass scaling for thin walled structures modeled with tri-linear solid elements. *Computational Mechanics* Jul 2004; **34**(2):134–136.

22. Wall WA, Gee M, Ramm E. The challenge of a three-dimensional shell formulation: the conditioning problem. *Proc. IASS-IACM 2000 Fourth International Colloquium on Computation for Shells & Spatial Structures*, 2000; 1–21.

23. Gee M, Ramm E, Wall W. Parallel multilevel solution of nonlinear shell structures. *Computer Methods in Applied Mechanics and Engineering* Jun 2005; **194**(21-24):2513–2533.

24. Klöppel T, Gee MW, Wall WA. A scaled thickness conditioning for solid- and solid-shell discretizations of thin-walled structures. *Computer Methods in Applied Mechanics and Engineering* Feb 2011; **200**(9-12):1301–1310.

25. Gershgorin S. Ueber die abgrenzung der eigenwerte einer matrix. *Izv. Akad. Nauk. SSSR Ser. Mat.(Bulletin de l'Academie des Sciences de l'URSS. Classe des sciences mathematiques et na)* 1931; **6**:749–754.

26. Flanagan DP, Belytschko T. Eigenvalues and Stable Time Steps for the Uniform Strain Hexahedron and Quadrilateral. *Journal of Applied Mechanics* 1984; **51**(1):35–40.

27. Hallquist JO. *LS-Dyna Theoretical Manual*. Livermore Software Technology Corporation, 2002.

28. Schwarze M, Reese S. A reduced integration solid-shell finite element based on the EAS and the ANS concept: Geometrically linear problems. *International Journal for Numerical Methods in Engineering* 2009; **80**(10):1322–1355.

29. Hinton E, Rock T, Zienkiewicz OC. A note on mass lumping and related processes in the finite element method. *Earthquake Engineering and Structural Dynamics* 1976; **4**(3):245–249.

30. Tkachuk A. Variational methods for consistent singular and scaled mass matrices. PhD Thesis, Stuttgart University 2013.

- When time step size has to be updated, for each element in the mesh:
- compute $\mathbf{J}_0$, $\mathbf{J}_0^{-1}$
- compute $\mathbf{c}_0^{1/\alpha} = \mathbf{J}_0^{-T}\mathbf{I}_3^{1/\alpha}\mathbf{J}_0^{-1}$
- compute invariants of $\mathbf{c}_0^{1/\alpha}$:

$$I_1^{1/\alpha} = [\mathbf{c}_0^{1/\alpha}]_{11} + [\mathbf{c}_0^{1/\alpha}]_{22} + [\mathbf{c}_0^{1/\alpha}]_{33}$$
$$I_2^{1/\alpha} = [\mathbf{c}_0^{1/\alpha}]_{11}[\mathbf{c}_0^{1/\alpha}]_{22} + [\mathbf{c}_0^{1/\alpha}]_{11}[\mathbf{c}_0^{1/\alpha}]_{33} + [\mathbf{c}_0^{1/\alpha}]_{22}[\mathbf{c}_0^{1/\alpha}]_{33} - [\mathbf{c}_0^{1/\alpha}]_{12}^2 - [\mathbf{c}_0^{1/\alpha}]_{13}^2 - [\mathbf{c}_0^{1/\alpha}]_{23}^2$$
$$I_3^{1/\alpha} = \det[\mathbf{c}_0^{1/\alpha}]$$

- compute Gershgorin estimate ω_G^2 of ω_{max}^2

$$\omega_{max}^2 \leq \omega_G^2 = \frac{2\mu}{\rho_0}\left[\frac{\nu}{1-2\nu}I_1^{1/\alpha} + \max_i\left\{\sum_{j=1}^3\left|[\mathbf{c}_0^{1/\alpha}]_{ij}\right|\right\}\right]$$

- compute residuum $f(\omega_G^2; \alpha^{opt})$ of characteristic polynomial for $\omega_{max}^2 = \omega_G^2$ and $\alpha = \alpha^{opt}$

$$f(\omega_G^2; \alpha^{opt}) = (\omega_G^2)^3 - \frac{1-\nu}{1-2\nu}\frac{2\mu}{\rho_0}I_1^{1/\alpha}(\omega_G^2)^2 + \frac{1}{1-2\nu}\left(\frac{2\mu}{\rho_0}\right)^2 I_2^{1/\alpha}\omega_G^2 - \frac{1+\nu}{1-2\nu}\left(\frac{2\mu}{\rho_0}\right)^3 I_3^{1/\alpha}$$

- compute new and final estimate (upper bound) of ω_{max}^2

$$\omega_{N-R}^2 \approx \omega_G^2 - \frac{f\left(\omega_G^2; \alpha^{opt}\right)}{f'\left(\omega_G^2; \alpha^{opt}\right)}$$

with

$$f'\left(\omega_G^2; \alpha\right) = 3(\omega_G^2)^2 - 2\frac{1-\nu}{1-2\nu}\frac{2\mu}{\rho_0}I_1^{1/\alpha}(\omega_G^2) + \frac{1}{1-2\nu}\left(\frac{2\mu}{\rho_0}\right)^2 I_2^{1/\alpha}$$

Box 1: Procedure for run-time element eigenfrequency computation.